PERTURBING IDEAL MAGNETOHYDRODYNAMIC STABILITY FOR TOROIDAL PLASMAS

by

Kate Comer

Faculty adviser: J.D. Callen

A dissertation submitted in partial fulfillment of the
requirements for the degree of

Doctor of Philosophy
(Nuclear Engineering and Engineering Physics)

at the
UNIVERSITY OF WISCONSIN—MADISON
August 2004

Perturbing Ideal Magnetohydrodynamic Stability for Toroidal Plasmas

Kate Comer

Under the supervision of Professor James D. Callen

At the University of Wisconsin-Madison

We have introduced a new perturbative technique with the goal of rapidly exploring the dependence of long wavelength ideal magnetohydrodynamic (MHD) instabilities on equilibrium profiles, shaping properties, and wall parameters. Traditionally, these relations are studied with numerical parameter scans using computationally intensive stability codes. Our perturbative technique first finds the equilibrium and stability using traditional methods. Subsequent small changes in the original equilibrium profiles, shaping properties, and wall parameters result in a new stability for the perturbed conditions. We quickly find the new stability with an expansion of the energy principle, rather than with another complete run of the stability codes.

We first apply the technique to semi-analytic screw pinch equilibria. The screw pinch results validate the approach, but also indicate that equilibria with certain features allow only very small perturbations.

Next, we extend the approach to toroidal geometry using experimental equilibria and a simple constructed equilibrium, with the ideal MHD stability code GATO. Stability properties are successfully predicted from perturbed toroidal equilibria when only the vacuum beyond the plasma is perturbed (through wall parameter variations), rather than the plasma itself. Small plasma equilibrium perturbations to both the experimental and simple equilibria result in very large errors to the predicted stability, and results are valid only over a narrow range of most perturbations.

The unexpected sensitivity to equilibrium (rather than wall) perturbations is due

to the compressional Alfvén energy contribution to the stability. Beyond a very small range of perturbations, second order terms in the expansion of the compressional Alfvén energy become large. We explore several methods of ameliorating these second order terms, but none improve results consistently or in a meaningful way.

Despite the large errors produced when changing plasma parameters, the wall perturbations revealed two useful applications of this technique. Because the central calculations are non-iterative matrix multiplications, there are none of the convergence issues that can disrupt a full MHD stability code. Marginal stability, therefore, is much easier to find with the perturbative technique. Also, the perturbed results can be input as the initial guess for the eigenvalue to full stability code, and improve subsequent convergence.

To Mom and Marc. I love you.

"Blessed are those who live out their dreams."

-Frank Sanders

Acknowledgements and thanks

I appreciate the guidance and patience of my thesis advisers Jim Callen and Chris Hegna, and mentor Alan Turnbull at General Atomics. Alan has always made me welcome in San Diego and made my visits productive. Thanks also to Steve Cowley at UCLA for the initial idea that grew into this thesis, and Carl Sovinec for insightful comments and computational help.

I also appreciate sponsorship from the UW, my Department, the U.S. Department of Energy (DOE) via the Fusion Energy Sciences fellowship, the Graduate School through the K-through-Infinity teaching fellowship, and the generous support of Jim Callen.[1]

Thanks to all of my friends and family for their encouragement, love and occassional kick in the pants. Special thanks to Madelyn and John Comer, Gloria Luppens, Katy Reedy and Tim Stankevitz, Scott and Peggy Kruger, Barb Griffith, Brad Binder, Lizzie Aldag and Holly Jellinek, Jasons Powell and Rood, and Frank Sanders for friendship, encouragement, and good examples. Sincere gratitude to Dr. Burton Kushner, for fixing my eyes. I really do not think I could have finished with the ones I had.

Heartfelt thanks to Ted Terpstra, Linda Casselman-Terpstra, and Alexandra Buckingham. My experiences at GA would not have been as fruitful and rich, or even possible, without them welcoming me into their family and home.

Finally, deepest gratitude to my mom Lydia Comer and my love Marc Christensen, for sharing the highs and lows and giving me confidence.

Kate Comer

University of Wisconsin-Madion, August 2004

[1] through DOE grants DE-FG02-86ER53218 and DE-FG02-92ER54139.

Contents

List of Figures

Chapter 1

Introduction

We are confronted with a rapidly increasing world energy demand due to growing world population and rising per capita energy consumption: the world's energy use is expected to triple in 50 years [1]. Fossil fuels cannot be expected to meet this demand long-term. One possible option to satisfy our future energy needs is magnetic fusion, which has some distinct advantages:[1]

- Fusion reactors are inherently passively safe.
- Environmental impacts are lower: there is no direct radioactive waste, indirect waste from reactor activation should be a manageable burden, and there are no combustion gasses to contribute to acid rain, ozone depletion, or the greenhouse effect.

An obvious disadvantage of fusion energy is that it has not yet been demonstrated in a pilot reactor. High plasma pressure, good plasma confinement, and steady state operation with a modest magnetic field in a single, economic reactor is the ultimate goal of magnetic fusion research. To attain this goal, plasma equilibrium, stability, and heat and mass transport must be adequately understood and controlled. Here we focus on ideal magnetohydrodynamic (MHD) stability.

[1]Reference [1] contains more details.

As theories have progressed and reactor designs have become more complex, researchers have repeatedly been frustrated by a mundane limitation: macroscopic MHD stability codes can take a long time to run, even with the advances in computing hardware and parallelization. In the best cases, an ideal MHD code analyzing a high aspect ratio plasma at high resolution[2] takes at least 2–3 hours to complete on today's computers. Extremely shaped or low aspect ratio geometries, which seem to lead to higher plasma pressure operating regimes, can take several times longer. Because of the time involved, parameter scans to determine, for instance, the most stable shaping factors for given pressure and current profiles are limited to examining only a few values.

Reducing the time required for parameter scans would facilitate thorough design studies. In-depth parameter scans, especially for large experiments such as the International Tokamak Experimental Reactor (ITER), require so many runs that a study of sufficient detail could take years. A tool that could fill in some of the points in parameter space with tens rather than hundreds of stability code runs should make parameter studies more thorough and easier to perform.

Stability computations for low aspect ratio equilibria are especially demanding. The large triangularity and strong toroidicity of these plasmas result in very high magnetic winding number q ($\sim$10–20) and magnetic shear near the edge. The high edge q and shear require a large number of finite elements and poloidal harmonics for accurate computation of low-n instability growth rates. Looked at another way, high magnetic field line pitch in the outer region of low aspect ratio plasmas causes a straight field line coordinate system to have poorer resolution in this region.

Typical stability calculations might use a $\psi \times \theta$ grid of 100×200 on the plasma cross-section. Low aspect ratio computations easily require 200×200 to 200×500

[2]Here, high resolution means a 200 x 400 computational mesh on the plasma cross-section.

grid points. Usually, for analyses of equilibria with conventional aspect ratio and with $n \leq 3$ modes, $\sim$30 poloidal harmonics are required. Low aspect ratio plasmas can easily require 50–80 poloidal harmonics.[3] Convergence studies, which ascertain when results do not unexpectedly change as the number of grid points or poloidal harmonics increases, also take longer for low aspect ratio equilibria.

Eigenmode details also increase with low aspect ratio. Using the stability code GATO [3], Turnbull *et al.* reported that toroidal coupling between toroidal Alfvén eigenmodes (TAEs) and continuum branches split the TAEs, and also found a new, second-order TAE [4]. Multiple TAEs at low aspect ratio were also analyzed by Candy *et al.* and reported by Holties *et al.*[5, 6].

Computational demands are not limited to physically large or low aspect ratio designs. Researchers frequently limit the scope of their studies for no reason other than computation time. An example is Holties *et al.*'s study of infernal modes using JET geometry [7]. Holties *et al.* required hundreds of runs of the stability code CASTOR [8] to estimate the effects of varying the pressure profile, q profile shape, and q_{min} — and he explicitly states that only a simple shape (an up-down symmetric D shape without X points) was considered to reduce calculation time. A faster perturbed stability code, which is the goal of this thesis, might have allowed the current profile, boundary conditions, resistivity, and shape to be varied as well.

Holmes *et al.*'s optimization study using the stability code PEST [9] provides another example of limited scope [10]. The computational requirements of PEST prevented Holmes *et al.* from examining the cumulative effects of parameter changes: he

[3] As a rule of thumb, the number of poloidal harmonics is less than $nq_{edge} + 25$ for low n mode numbers and an equal-arc-length Jacobian [2].

varied q and pressure profiles while holding the aspect ratio, triangularity, and elongation constant. Thorough optimization would require examining different shapes while varying the profiles, as was done for DIII-D [11].

The goal of this research is not to reduce the time to run a stability code for a specific set of parameters, but to speed up stability predictions for variations on a particular *set* of parameters. Determining the stability properties of a single specific equilibrium still takes just as long, but we have tried to relatively quickly estimate the stability of several similar equilibria. In theory, one should be able to predict changes in macroscopic ideal MHD stability that are caused by slight perturbations to the parameters defining the plasma equilibrium.

The general theory and computational steps involved in finding stability conditions of perturbed equilibria are outlined only briefly here, but are detailed in Chapter 2:

1. Obtain a force-balance equilibrium and the stability properties for an initial set of parameters.

2. Perturb the initial set of parameters.

3. Obtain a new perturbed equilibrium with the perturbed parameters.

4. Combine the initial stability properties and perturbed equilibrium in the perturbed energy principle.

5. Solve the perturbed energy principle for the perturbed stability.

The equations for a screw pinch can be solved analytically, and we examined this geometry first. Chapter 3 discusses the reasons for this approach, and the analytic results. In general, perturbing screw pinch equilibria led to accurate stability predictions.

Predicting stability properties of perturbed toroidal equilibria must be done numerically. Both experimental and idealized equilibria were perturbed. Stability properties were successfully predicted from perturbed toroidal equilibria in one particular instance: when only the vacuum beyond the plasma was perturbed (through wall parameter perturbations), rather than the plasma itself. When other parameters were varied beyond a very narrow range of perturbations, the predicted stability consistently contained a large, rapidly growing error. Chapter 4 examines these toroidal equilibria. Chapter 5 investigates possible sources of the error, and discusses attempts (largely unsuccessful) to reduce it. Finally, Chapter 6 summarizes the conclusions of this study and the situations best suited for the perturbative technique.

Chapter 2

Perturbations of the Energy Principle and Initial Equilibrium

2.1 The energy principle

Traditionally, the linear ideal magnetohydrodynamic (MHD) stability of a plasma in force-balance equilibrium is determined through an energy principle, which gives the change in the potential energy (δW) caused by plasma displacements ($\underline{\xi}$) against forces ($\underline{F}$) in the plasma [12]:

$$\begin{aligned} \delta W(\underline{\xi}, \underline{\xi}^*) &= -\tfrac{1}{2} \int \underline{\xi}^* \cdot \underline{F}(\underline{\xi}) \; d^3r \\ work &= distance \cdot force. \end{aligned} \tag{2.1}$$

For stability, $\delta W > 0$. If a plasma is displaced by a quantity $\underline{\xi}$ away from stability, the displacement behaves as $e^{-i\omega t}$, with $\omega^2 = \dfrac{\delta W}{K}$, where K is the kinetic energy associated with the displacements:

$$K(\underline{\xi}, \underline{\xi}^*) = \tfrac{1}{2} \int \rho |\underline{\xi}|^2 \; d^3r \tag{2.2}$$

Positive δW results in oscillations, while negative δW results in exponential growth and decay.

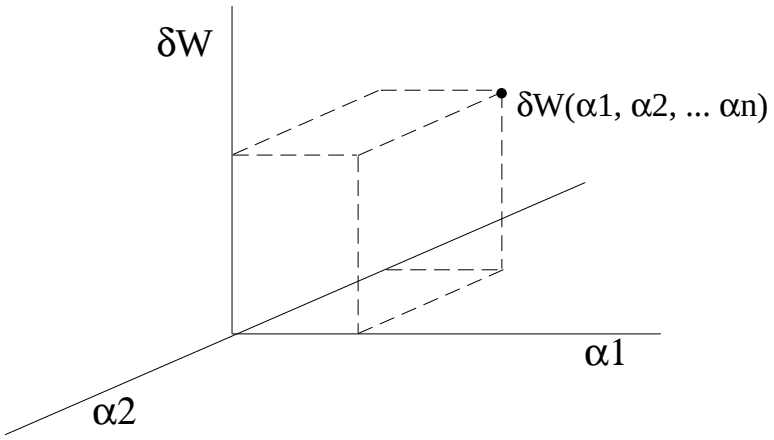

Figure 2.1: Computational results give a single point in α-parameter space.

Stability predictions begin with a plasma in force-balance equilibrium defined by boundary conditions and a set of parameters $\underline{\alpha}(\alpha_1, \alpha_2, \alpha_3...)$. The parameters can be, for example, shaping factors, or profiles for the pressure p, current density $\underline{J}$, magnetic field winding number q, or magnetic field $\underline{B}$. A stability code determines the plasma displacements by applying variational calculus to the energy principle:

$$\Delta\delta W = -\tfrac{1}{2}\int \left[\delta\underline{\xi}^* \cdot \underline{F}(\underline{\xi}_{min}) + \underline{\xi}^*_{min} \cdot \underline{F}(\delta\underline{\xi})\right]\ d^3r = 0. \tag{2.3}$$

Proper selection of the displacements $\underline{\xi}_{min}$ minimize the energy principle, giving $\Delta\delta W = 0$. The force operator $\underline{F}$ is defined by the equilibrium and depends on the parameters $\underline{\alpha}$. The boundary conditions are contained in $\int d^3r$. These results give one point in parameter-space, as illustrated in Figure 2.1. Values for $\underline{\xi}$ and δW can be found analytically for only the simplest equilibria. Computationally, stability codes minimize the energy principle by solving the eigenvalue problem $A\underline{x} = \omega^2 B\underline{x}$, where $A\underline{x}$ and $B\underline{x}$ are matrices representing the potential and kinetic energies, and the eigenvector $\underline{x}$ represents the displacements.

2.2 Perturbing the energy principle

So far, the method presented is standard procedure for computing the stability properties of a single equilibrium. Next, the equilibrium parameters are changed slightly: $\underline{\alpha} \to \underline{\alpha} + \Delta\underline{\alpha}$. This could be, for example, a change in the pressure profile: $p \to p + \Delta p$.

Changing the parameters causes a change in the energies and stability properties:

$$\begin{aligned} \omega^2 &\to \omega^2 + \Delta\omega^2, & \underline{\xi} &\to \underline{\xi} + \Delta\underline{\xi}, \\ \delta W &\to \delta W + \Delta\delta W, & K &\to K + \Delta K. \end{aligned} \tag{2.4}$$

We now expand $\omega^2 = \dfrac{\delta W}{K}$. We use the self-adjointness of $\underline{F}$ (described in [12]) to make the following substitutions:

$$\int \left[\Delta\underline{\xi}^* \cdot \underline{F}(\underline{\xi}) + \underline{\xi}^* \cdot \underline{F}(\Delta\underline{\xi})\right] \, d^3r = 2\int \Delta\underline{\xi}^* \cdot \underline{F}(\underline{\xi}) \, d^3r \tag{2.5}$$

$$\int \left[\Delta\underline{\xi}^* \cdot \Delta\underline{F}(\underline{\xi}) + \underline{\xi}^* \cdot \Delta\underline{F}(\Delta\underline{\xi})\right] \, d^3r = 2\int \Delta\underline{\xi}^* \cdot \Delta\underline{F}(\underline{\xi}) \, d^3r. \tag{2.6}$$

With these substitutions, $\omega^2 = \dfrac{\delta W}{K}$ is expanded as:

$$\begin{aligned} \omega^2 + \Delta\omega^2 = -\tfrac{1}{2}\int d^3r \, \big[&\underline{\xi}^* \cdot \underline{F}(\underline{\xi}) + \Delta\underline{\xi}^* \cdot \underline{F}(\Delta\underline{\xi}) + 2\Delta\underline{\xi}^* \cdot \underline{F}(\underline{\xi}) + \underline{\xi}^* \cdot \Delta\underline{F}(\underline{\xi}) \\ &+ 2\Delta\underline{\xi}^* \cdot \Delta\underline{F}(\underline{\xi}) + \Delta\underline{\xi}^* \cdot \Delta\underline{F}(\Delta\underline{\xi})\big] \quad / \\ \tfrac{1}{2}\int d^3r \, &\left[\rho|\underline{\xi}|^2 + \Delta\rho|\underline{\xi}|^2 + 2\rho|\underline{\xi} \cdot \Delta\underline{\xi}| + 2\Delta\rho|\underline{\xi} \cdot \Delta\underline{\xi}| + \rho|\Delta\underline{\xi}|^2 + \Delta\rho|\Delta\underline{\xi}|^2\right]. \end{aligned} \tag{2.7}$$

After some algebraic manipulation, we can use the equation of motion to cancel the self-adjoint terms that are first order in $\Delta\underline{\xi}$:

$$(2\omega^2)2K(\rho, \underline{\xi}, \Delta\underline{\xi}) - 2\Delta\underline{\xi}^* \cdot \underline{F}(\underline{\xi}) = 0. \tag{2.8}$$

The denominator can be further simplified. We write the denominator as $\rho|\underline{\xi}|^2(1+\epsilon)$, with

$$\epsilon = \frac{\Delta\rho|\underline{\xi}|^2 + 2\rho|\underline{\xi} \cdot \Delta\underline{\xi}| + 2\Delta\rho|\underline{\xi} \cdot \Delta\underline{\xi}| + \rho|\Delta\underline{\xi}|^2 + \Delta\rho|\Delta\underline{\xi}|^2}{\rho|\underline{\xi}|^2}. \tag{2.9}$$

Next, we estimate $1/(1+\epsilon) \approx 1-\epsilon$. When the resulting second and third order terms are neglected, we can numerically find $\Delta\omega^2$, the change in the stability eigenvalue induced by perturbing the equilibrium parameters:

$$\Delta\omega^2 \approx \frac{-\frac{1}{2}\int d^3r\ \underline{\xi}^* \cdot \Delta\underline{F}(\underline{\xi}) - \omega^2\Delta\rho|\underline{\xi}|^2}{\frac{1}{2}\int d^3r\ \rho|\underline{\xi}|^2}. \tag{2.10}$$

When $\Delta\rho/\rho$ is also neglected, we obtain the perturbed potential energy:

$$\Delta\delta W = -\tfrac{1}{2}\int \underline{\xi}^* \cdot \Delta\underline{F}(\underline{\xi})\ d^3r. \tag{2.11}$$

The perturbed force $\Delta\underline{F}$ contains the changes in $\underline{\alpha}$. For ideal MHD, $\underline{F}$ is commonly expressed as [12]:

$$\underline{F} = \frac{1}{\mu_0}(\nabla\times\underline{B}_0)\times\left[\nabla\times(\underline{\xi}\times\underline{B}_0)\right] + \frac{1}{\mu_0}\left[\nabla\times\left(\nabla\times(\underline{\xi}\times\underline{B}_0)\right)\right]\times\underline{B}_0 + \nabla(\underline{\xi}\cdot\nabla p + \gamma p\nabla\cdot\underline{\xi}) \tag{2.12}$$

where $\underline{B}_0$ is equilibrium magnetic field, p is equilibrium pressure, and γ is the adiabatic exponent of $\frac{5}{3}$. An interesting future extension to $\Delta\underline{F}$, useful for internal kink modes at high temperature, might be including a thermal trapped particle kinetic term, as was done, for example, for large aspect ratio, circular tokamaks by Antonsen and Bondeson [13].

The force $\underline{F}$ is also a function of the poloidal flux ψ, which is also used as a "radial" equilibrium coordinate. We initially determine ψ by solving the Grad-Shafranov equilibrium equation [12]:

$$\begin{aligned} \Delta^*\psi &= -\mu_0 R^2 p' - FF', \\ \Delta^* &= R\frac{\partial}{\partial R}\left(\frac{1}{R}\frac{\partial\psi}{\partial R}\right) + \frac{\partial^2\psi}{\partial Z^2}. \end{aligned} \tag{2.13}$$

To use consistent coordinates in the perturbed calculations, we find $\psi_{perturbed}$ by re-solving the Grad-Shafranov equation with the perturbed quantities. Many Grad-Shafranov equilibrium equation solvers have been developed to numerically solve for ψ

(for example, EFIT [14], Tokamac [15], TOQ [16, 17], CHEASE [18], JSOLVER [19]). We use experimental equilibria available in EFIT format, and generate ideal equilibria using TOQ.

Once $\psi_{original}$ and $\psi_{perturbed}$ are obtained, Equation (2.11) can be solved for $\Delta\delta W$:

$$\begin{aligned} \Delta\delta W &= -\tfrac{1}{2}\int \underline{\xi}^*_{min} \cdot \Delta\underline{F}(\psi_{original}, \psi_{perturbed}, \underline{\xi}_{min})\ d^3r, \\ \Delta\underline{F} &= \underline{F}_{perturbed}(\alpha+\Delta\alpha, \psi_{perturbed}) - \underline{F}_{original}(\alpha, \psi_{original}) \end{aligned} \tag{2.14}$$

with $\underline{\xi}_{min}$ from the stability code results, and the perturbations $\Delta\underline{\alpha}$ contained in the integral bounds, $\Delta\underline{F}$, and $\psi_{perturbed}$.

2.3 Numeric considerations

In practice, to find δW from perturbed toroidal equilibria we rely on results from the numerical stability code GATO [3]. Equations (2.11) and (2.12) are rewritten to reflect the coordinate system and benefit from the computational efficiencies used in GATO:

$$\begin{aligned} \Delta\delta W &= \delta W_{perturbed} - \delta W_{initial} \\ \Delta\delta W &= -\tfrac{1}{2}\int_{perturbed} \underline{\xi}^*_{initial} \cdot \underline{F}_{perturbed}(\underline{\xi}_{initial})\ d^3r \\ &\quad +\tfrac{1}{2}\int_{initial} \underline{\xi}^*_{initial} \cdot \underline{F}_{initial}(\underline{\xi}_{initial})\ d^3r \end{aligned} \tag{2.15}$$

For consistency, the same convention is used in the screw pinch analysis. The new, perturbed $\delta W_{perturbed}$ is calculated using $\underline{\xi}_{initial}$ (the displacements from the initial stability results) and $\underline{F}_{perturbed}$ determined from the new equilibrium. Only *parameters* defining the equilibrium have been directly perturbed. Neither the equilibrium solution nor $\underline{F}_{perturbed}$ have undergone a simple direct perturbation. The new equilibrium is completely recalculated, based on the perturbed parameters. Also, $\underline{F}_{perturbed}$ is completely

recalculated based on the new recalculated equilibrium. The subscript *perturbed* on $\underline{F}_{perturbed}$ refers to perturbing the underlying parameters, not perturbing $\underline{F}$ itself.

The change $\Delta\delta W$ we are interested in is the difference between $\delta W_{perturbed}$ and the originally computed $\delta W_{initial}$. To preserve the information available in both potential energies, results in Chapter 4 will show both $\delta W_{perturbed}$ and $\delta W_{initial}$ rather than $\Delta\delta W$ alone.

Computing $\delta W_{perturbed}$ in addition to $\Delta\delta W$ alone also allows further examination of energy terms. As will be seen in Chapter 4, estimates of $\Delta\delta W$ are generally not very good for toroidal equilibria. Examining the various components of δW helps determine the source of errors, though some forms of δW are more helpful than others.

It is most useful to examine δW_{plasma} in the form first given by Furth, Killeen, Rosenbluth and Coppi [20], and later modified by Greene and Johnson [21] and Bateman [22]. In this form every component of the plasma energy has physical meaning:

$$\delta W = \delta W_{plasma} + \delta W_{vacuum}$$

$$\delta W_{plasma} = \frac{1}{2}\int_{plasma} d^3r \left(\underbrace{\mu_0 \left| \frac{1}{\mu_0}\underline{B}_{\|} - \frac{\underline{B}_0 \underline{\xi}\cdot\nabla p}{|B_0|^2} \right|^2}_{\text{compressional Alfvén}} + \underbrace{\frac{1}{\mu_0}|\underline{B}_{\perp}|^2}_{\text{shear Alfvén}} + \underbrace{\gamma p |\nabla\cdot\underline{\xi}|^2}_{\text{acoustic}} \right.$$

$$\left. + \underbrace{\frac{(J_0\cdot B_0)}{|B_0|^2}\underline{B}_0 \times \underline{\xi}\cdot\underline{B}}_{\text{current-driven kink}} - \underbrace{2(\underline{\xi}\cdot\nabla p)(\underline{\xi}\cdot\kappa)}_{\text{pressure-driven interchange}} \right). \qquad (2.16)$$

Rather than using this form of δW, GATO uses a form that facilitates computation in an axisymmetric coordinate system. The coordinates are: the toroidal angle ϕ, poloidal flux $2\pi\psi$ as the radial coordinate, and an arbitrary poloidal coordinate χ selected to optimize grid mapping. In general terms, δW is represented in GATO as:

$$\delta W = \delta W_{plasma} + \delta W_{vacuum}$$

$$\delta W_{plasma} = \delta W_{destabilizing} + \delta W_{B_\psi} + \delta W_{B_\chi} + \delta W_{B_\phi} + \delta W_{compressional}. \qquad (2.17)$$

Some of these terms correspond very well to those of the "intuitive" form of δW given in Equation (2.16). The radial magnetic field line bending energy term, δW_{B_ψ}, corresponds roughly to the shear Alfvén term of Equation (2.16). The compressional term is the same as the acoustic term of Equation (2.16). The destabilizing term contains some, but not all of the current-driven kink and pressure-drive interchange terms of Equation (2.16). The remaining poloidal and toroidal magnetic field line bending energy terms, δW_{B_χ} and δW_{B_ϕ}, together contain the compressional Alfvén term and the remaining parts of the current-driven kink and pressure-drive interchange terms.

2.4 Coordinate system consistency

When δW is found semi-analtically, as for the screw pinch, equilibrium quanities (current, pressure, q) and displacements $\underline{\xi}$ are continuous radial functions. There is no shift in the coordinate system when the equilibrium is perturbed.

In contrast, computational stability codes, including GATO, usually generate new coordinate systems for new equilibria. Equilibrium quantities and displacements are discretized according to the finite elements representation used by the code, and changing the equilibrium generally results in a subtle modification of the basis functions used to define the computational mesh. Here we first describe the representation used in GATO, and then explain the precautions we have taken to avoid this shift.

Although GATO is based on (ϕ, ψ, χ) coordinates, the problem is first re-cast with

the contravariant components X, U, and Y:

$$\begin{aligned} X &= J|\nabla\psi|\xi_s/r^2, \\ U &= 2s\psi_s\xi_\chi/r|\nabla\psi| - Y + \beta_\chi X, \\ Y &= 2s\psi_s\xi_\phi/I_p r, \end{aligned} \tag{2.18}$$

where $s = \sqrt{\psi/\psi_s}$ is the radial variable, ψ_s denotes the toroidal magnetic flux at the plasma surface, $J = qr^2/I_p$ is the Jacobian, I_p is the flux of the poloidal plasma current, and $\beta_\chi = [\partial\chi/\partial s]_\perp$ measures the non-orthogonality of the coordinate system [23].

The variables X, U, and Y are further expanded, so that instead of solving the variational Lagrangrian $\delta L(X,U,Y) = \delta(W - \omega^2 K) = 0$, GATO solves

$$\delta L\left(\frac{\partial X^{(1)}}{\partial\chi}, X^{(2)}, \frac{\partial X^{(3)}}{\partial s}, \frac{\partial U^{(1)}}{\partial\chi}, U^{(2)}, \frac{\partial Y^{(1)}}{\partial\chi}, Y^{(2)}\right) = 0. \tag{2.19}$$

The new variables are restricted by the identities

$$X^{(1)} = X^{(2)} = X^{(3)}, \quad U^{(1)} = U^{(2)}, \quad \text{and} \quad Y^{(1)} = Y^{(2)} \tag{2.20}$$

on specific points in each mesh cell. These variables are discretized on an i,j (radial, poloidal) mesh, and expanded in terms of the basis functions d_{ij}, e_{ij}, f_{ij}, $g_{i+1/2,j}$ and $h_{i+1/2,j}$:

$$\begin{aligned} X^{(1)} &= \sum_i\sum_j X_{ij}d_{ij}, \quad X^{(2)} = \sum_i\sum_j X_{ij}e_{ij}, \quad X^{(3)} = \sum_i\sum_j X_{ij}f_{ij}, \\ U^{(1)} &= \sum_i\sum_j U_{i+1/2,j}g_{i+1/2,j}, \quad U^{(2)} = \sum_i\sum_j U_{i+1/2,j}h_{i+1/2,j}, \\ Y^{(1)} &= \sum_i\sum_j Y_{i+1/2,j}g_{i+1/2,j}, \quad \text{and} \quad Y^{(2)} = \sum_i\sum_j Y_{i+1/2,j}h_{i+1/2,j}. \end{aligned} \tag{2.21}$$

Choosing these components and specific basis functions satisfies particular conditions that allow solutions for marginal stability ($\omega^2 = 0$), in particular $\underline{\nabla}\cdot\underline{\xi} = 0$. The stable

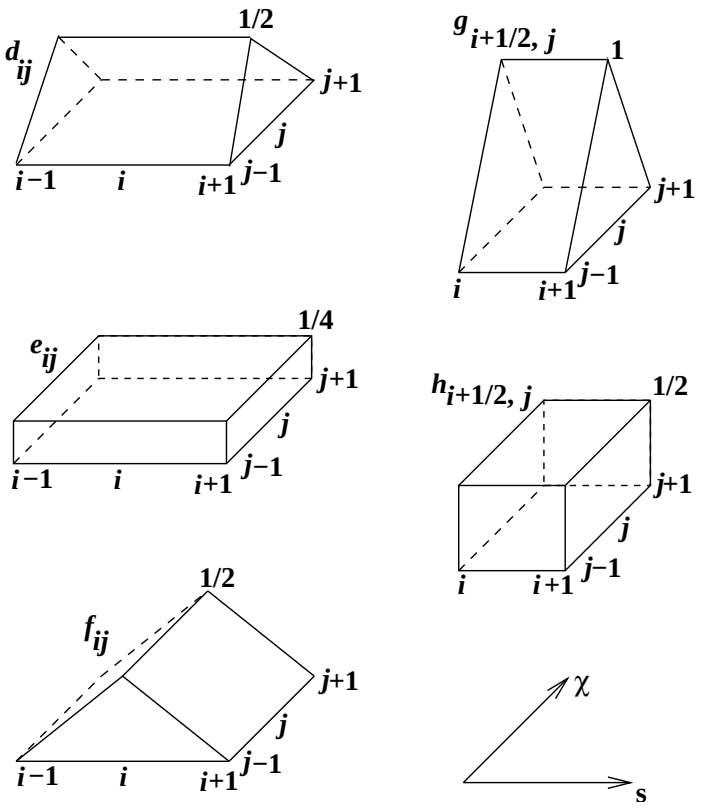

Figure 2.2: Basis functions for the expansions of the variables $X^{(1)}$ (d_{ij}), $X^{(2)}$ (e_{ij}), $X^{(3)}$ (f_{ij}), $U^{(1)}$ $(g_{i+1/2,j})$, $U^{(2)}$ $(h_{i+1/2,j})$, $Y^{(1)}$ $(g_{i+1/2,j})$, and $Y^{(2)}$ $(h_{i+1/2,j})$.

and unstable parts of the λ-spectrum may then be separated, discrete solutions isolated from the continuous spectrum, and spectral pollution eliminated [23, 24].

The basis functions are shown in Figure 2.2. As they appear in the Lagrangian, all functions and their derivatives are piecewise constant. The equilibrium is also piecewise constant. The Lagrangian, therefore, appears as a finite difference problem, with necessary coefficients obtained from equilibrium values at the center of each cell.

To avoid any change in the basis functions, we have chosen to test our $\Delta\delta W$ method only with perturbations that do not change the distribution of mesh points, the mapping (from the equilibrium mesh to the stability calculation mesh) or the stability

calculation mesh. The analysis of Section 2.2 did not address basis functions. In particular, Equations 2.10 and 2.11 would generally need to reference basis functions. Because we are careful not to change the coordinate system, Equation (2.15) may be used. We will confirm this assertion in later chapters.

2.5 Similar techniques by others

Our approach for estimating stability by perturbing an equilibrium shares some characteristics with the analysis performed by Greene and Chance for the second region of ballooning stability [25], with Mercier and Luc's [26] and Miller *et al.*'s [27] local equilibrium models, and with Hegna and Nakajima's [28] and Hudson *et al.*'s [29] ballooning stability perturbations.

Before Greene and Chance's analysis, calculations for the second region of stability used equilibria obtained for the first stability (low-pressure) region. Since the high pressure of the second region of stability causes large distortions of the equilibrium, these first-region equilibria are not entirely appropriate. Greene and Chance, recognizing that ballooning stability is associated with localized pressure gradients and shear, recalculated the stability by:

1. obtaining an equilibrium for the first region,

2. introducing large but highly localized perturbations in the p and q profiles, and

3. applying these local perturbations to the equilibrium and ballooning equations.

The final equation for ballooning stability contained the original unperturbed profiles and two perturbed gradients localized at ψ_b: $p'^{(1)}(\psi_b)$ and $q'^{(1)}(\psi_b)$.

Mercier and Luc developed a local model for finite aspect ratio, non-circular equilibria [26]. Miller *et al.* extended this model by introducing a parameterization of the poloidal magnetic field [27]. The final model allows local perturbations of the global magnetic shear and pressure gradient, global perturbations of the elongation, triangularity and aspect ratio, and variations of the elongation, triangularity and major radius of a flux surface. These models have been used in ballooning mode studies [30, 27] and calculations of trapped particle precession [31], and extended to stellarator geometries [28].

Hegna and Nakajima [28], and Hudson *et al.* [29] performed a semi-analytic perturbation exercise for ballooning growth rates, with application to stellarators. After solving the ballooning eigenvalue equation with a particular pressure gradient p' and averaged magnetic shear ι', both p' and ι' were perturbed at an arbitrary flux surface. A new value for the growth rate λ was found from a perturbation expansion:

$$\lambda(\delta p', \delta \iota') = \lambda_0 + \frac{\partial \lambda}{\partial p'} \delta p' + \frac{\partial \lambda}{\partial \iota'} \delta \iota' + \cdots. \tag{2.22}$$

In both our method and this method, a single growth rate calculation is used to find the growth rates for an entire family of equilibria. Hudson's method, however, is limited to infinite-n ballooning modes, and the domain is computationally simplified to a single magnetic field line.

Our approach extends the analyses of Greene and Chance, Mercier and Luc, Miller *et al.*, Hegna and Nakajima, and Hudson *et al.* in several important respects:

- The perturbations need not be localized,
- The results are not limited to ballooning modes, and
- More parameters can be varied.

Chapter 3

Perturbations of Screw Pinch Equilibria and Stability

The perturbation technique described in Chapter 2 depends on detailed equilibria and stability results, which are obtained numerically for reactor-relevant two-dimensional configurations. Before adding complications that might arise from such plasmas, we first determine if the approach is valid with the simpler one-dimensional geometry of the circular screw pinch, shown in Figure 3.1.

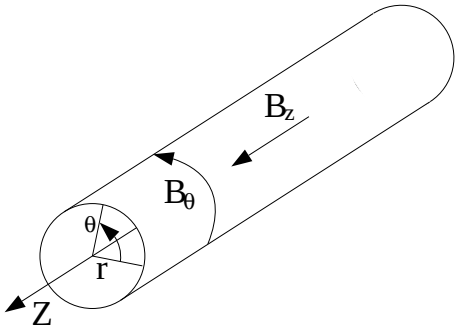

Figure 3.1: Screw pinch geometry with major radius = R and $2\pi R$ periodicity in the z direction.

The screw pinch allows variation only in the radial direction. The geometry of the screw pinch offers a simplified pressure profile and a simple relation between current density and magnetic field, and can be treated semi-analytically.

By starting with the screw pinch, we hope to obtain some insight into issues that

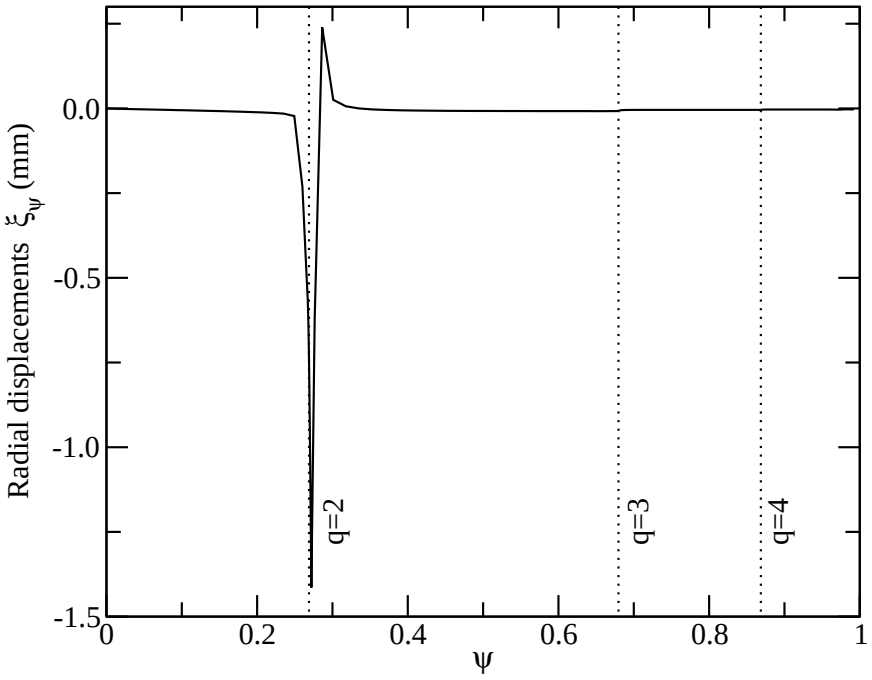

Figure 3.2: Real radial displacements along the plasma midplane for a toroidal internal $m/n = 2/1$ kink mode are localized at the $q = 2$ rational surface.

might also arise with an axisymmetric toroidal geometry. In this section we describe some of these potential issues. The rest of the chapter will then examine their manifestation for various equilibrium perturbations.

Internal modes, particularly $m/n = 1/1$, might not respond well to perturbation (m and n are the poloidal and toroidal mode numbers). Internal m/n kink modes commonly have displacements localized in distinct regions of the plasma where $q \approx m/n$, as shown in Figure 3.2. For $m/n = 1/1$ modes, displacements commonly abruptly change where q crosses 1, as shown in Figure 3.3.

In these initial configurations that have sharply localized displacements or displacements that abruptly drop to nearly zero, perturbing the equilibrium parameters might result in a change in q that should correspond to a significant change in displacements

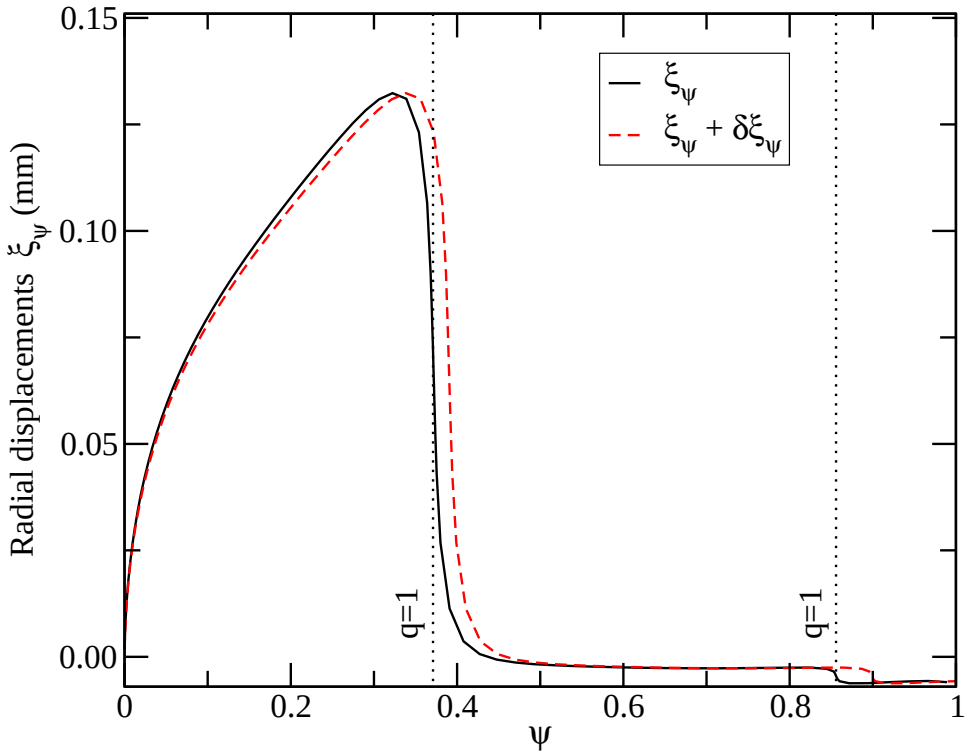

Figure 3.3: Real radial displacements along the plasma midplane for a toroidal $m/n = 1/1$ mode change abruptly at the $q = 1$ rational surface ($q > 1$).

for at least some of the plasma. For example, with an $m/n = 1/1$ mode, the $q = 1$ surface of a perturbed equilibrium could move away the center, as indicated by $\xi_\psi + \delta\xi_\psi$ in Figure 3.3. The actual displacements for the perturbed equilibrium would then extend over more of the plasma, compared to the initial equilibrium. Because the perturbed stability is computed with the *initial* displacements, the calculation would use no displacements in a small region that would have had large displacements if the stability results had been completely recalculated. One solution to this potential problem is basing the computational grid on the q-profile rather than on flux surfaces. Recalculating the displacements is *not* the solution — the essence of the perturbation technique is avoiding that time-intensive calculation.

There is also concern that single-fluid ideal MHD does not adequately describe the internal kink mode when the ion Larmor radius exceeds the scale length of the plasma displacements. This situation may be better described by a kinetic model or the two-fluid linear MHD description by Zakharov and Rogers [32].

There may also be an experimental limit on q near the edge, such as those observed on START (Small Tight Aspect Ratio Tokamak) [33]. Changing the parameters so that q violates that limit may give invalid perturbation results. Again, using a grid based on either flux surfaces or the q-profile as appropriate might be helpful.

Both the $m/n = 1/1$ mode and edge q complications are related to a larger question: how big can $\Delta\underline{\alpha}$ be? In general, the answer depends on the initial equilibrium. By first examining the screw pinch analytically, we answer some of these questions before they are complicated by a full toroidal geometry.

3.1 Initial screw pinch equilibria and parameters

Because of the symmetry of the screw pinch, the Grad-Shafranov equation is not needed to determine the equilibrium profiles. Combining Ampere's Law:

$$\mu_0 \underline{J} = \underline{\nabla} \times \underline{B} \Longrightarrow \tag{3.1}$$

$$\mu_0 J_\theta(r) = -\frac{d}{dr} B_z(r), \tag{3.2}$$

$$\mu_0 J_z(r) = \frac{1}{r}\frac{d}{dr} B_\theta(r), \tag{3.3}$$

with the radial force balance equation:

$$\underline{J} \times \underline{B} = \underline{\nabla} p \Longrightarrow \tag{3.4}$$

$$J_\theta(r) B_z(r) - J_z(r) B_\theta(r) = \frac{d}{dr} p(r), \tag{3.5}$$

yields

$$\frac{d}{dr}\left(p+\frac{{B^2}_z+{B^2}_\theta}{2\mu_0}\right)+\frac{{B^2}_\theta}{2\mu_0 r}=0. \tag{3.6}$$

We have three equations (3.2, 3.3, 3.6) and five unknown profiles ($J_\theta(r)$, $J_z(r)$, $B_\theta(r)$, $B_z(r)$ and $p(r)$), so can define two of the profiles. Although B_θ and B_z explicitly appear in Equation (3.6), p and J_z are commonly assigned rather than $\underline{B}$. We take current and pressure profiles from the literature ([2] and [34]), and define pressure and current profiles as:

$$J_z(r) = J_0\left[1-\left(\frac{r}{R_0}\right)^{\alpha_1}\right]^{\alpha_2}, \tag{3.7}$$

$$p(r) = p(0)\left[1-\left(\frac{r}{R_0}\right)^{\alpha_3}\right]^{\alpha_4}. \tag{3.8}$$

More detailed profiles from [35], [36], or [37] could have also been examined for the screw pinch. The profiles above, though, are flexible enough to both model very simple equilibria and approximate the experimental toroidal equilibria.

Determination of the displacements ξ with no wall surrounding the plasma generally follows the approach outlined in [12] and [38]. We find ξ by solving Newcomb's Euler-Lagrange equation:

$$0 = \frac{d}{dr}f\frac{d}{dr}\xi-g\xi, \tag{3.9}$$

$$f = \frac{rF^2}{{k_0}^2}, \tag{3.10}$$

$$g = 2\mu_0 p'\frac{k^2}{{k_0}^2}+rF^2\left(\frac{{k_0}^2r^2-1}{r^2{k_0}^2}\right)+ 2F\frac{k^2}{r{k_0}^4}\left(kB_z-\frac{mB_\theta}{r}\right),$$

$$F = \underline{k}\cdot\underline{B}=\frac{mB_\theta}{r}+kB_z, \tag{3.11}$$

$${k_0}^2 = k^2+\frac{m^2}{r^2}. \tag{3.12}$$

Here, k and m are the linear and azimuthal mode numbers used in a cylindrical geometry. They are analogous to the toroidal mode numbers n and m. In this formulation, contributions to δW from plasma compressibility have been analytically eliminated.

Using the equations given above, we examine several different types of free-boundary screw pinch equilibria, progressing from the simplest to more realistic:

- Flat pressure profile and flat current profile:

$$\begin{aligned} \alpha_2 &= 0 \implies J_z(r) = J_0, \\ \alpha_4 &= 0 \implies p(r) = p_0. \end{aligned}$$

  The pressure profile is perturbed by changing p_0.

- Curved pressure profile and flat current profile:

$$\begin{aligned} \alpha_2 &= 0 \implies J_z(r) = J_0, \\ \alpha_3 &= 2,\ \alpha_4 = 1 \implies p(r) = p_0 \left[1 - \left(\frac{r}{R_0}\right)^2\right]. \end{aligned}$$

  The pressure profile is perturbed by varying α_3 from 1.5 to 2.5.

- Flat pressure profile and piece-wise flat current profile with a step at $r = R_{step}$:

$$\begin{aligned} \alpha_2 &= 0 \implies J_z(r) = \begin{cases} J_0 & (r < R_{step}), \\ \alpha_5 J_0 & (r > R_{step}), \end{cases} \\ \alpha_4 &= 0 \implies p(r) = p_0. \end{aligned}$$

  The current profile is perturbed by varying α_5.

- Curved pressure profile and piece-wise flat current profile with a step at $r = R_{step}$:

$$\begin{aligned} \alpha_2 &= 0 \implies J_z(r) = \begin{cases} J_0 & (r < R_{step}), \\ \alpha_5 J_0 & (r > R_{step}), \end{cases} \\ \alpha_3 &= 2,\ \alpha_4 = 1 \implies p(r) = p_0 \left[1 - \left(\frac{r}{R_0}\right)^2\right]. \end{aligned}$$

As in the previous equilibrium, the current profile is perturbed by changing α_5.

- Curved pressure profile and curved current profile:

$$\begin{aligned} \alpha_1 &= 0,\ \alpha_2 = 1 \implies J_z(r) = J_0\left[1-\left(\frac{r}{R_0}\right)^2\right], \\ \alpha_3 &= 2,\ \alpha_4 = 1 \implies p(r) = p_0\left[1-\left(\frac{r}{R_0}\right)^2\right]. \end{aligned}$$

Either the current or pressure profile is perturbed by varying α_1 or α_3.

We examine both $m = 1$ and $m = 2$ modes. The curved profiles also allow exploration of equilibria with high edge shear.

3.2 Perturbation of screw pinch equilibria with constant pressure and constant current profiles

The first equilibrium we treat has constant pressure ($p/p_0 = 1$) and current ($J_z/J_0 = 1$). The perturbed equilibria are obtained by changing p/p_0 from 0.1 to 1.9. Using Equations (3.3 - 3.6) gives the magnetic field profiles:

$$\frac{B_\theta}{\mu_0 J_z} = \frac{r/R_0}{2}, \tag{3.13}$$

$$\frac{B_z}{B_0} = \sqrt{1 - \frac{r/R_0}{2}}, \tag{3.14}$$

$$B_0 = \frac{\mu_0 J_z}{2}\sqrt{3}. \tag{3.15}$$

Initial and perturbed profiles are shown in Figure 3.4. Because pressure is constant, $dp/dr = 0$ and $\underline{B}$ is not affected by the pressure perturbations.

First $\underline{\xi}$ and δW are found for the original equilibrium, for both $k/m = 1/1$ and $k/m = 1/2$. Next δW is found for the perturbed equilibria using the same $\underline{\xi}$. For comparison, the new ξ and corresponding δW are also found for each perturbed equilibrium.

Figure 3.5 compares the perturbed δW (using the original $\underline{\xi}$) and the fully computed δW (using the new $\underline{\xi}$) for each perturbed equilibrium for $k/m = 1/1$. Figure 3.6 shows the results for $k/m = 1/2$. In both cases, the perturbed and complete δW calculations agree very well over the entire range of pressure perturbations.

As a check on the calculation, we note that the decrease in δW with decreasing pressure observed in Figures 3.5 and 3.6 agrees with theory. The relevant term in δW is related to the compressional acoustic energy:

$$\delta W_{acoustic} = \gamma p_o |\underline{\nabla} \cdot \underline{\xi}|^2. \tag{3.16}$$

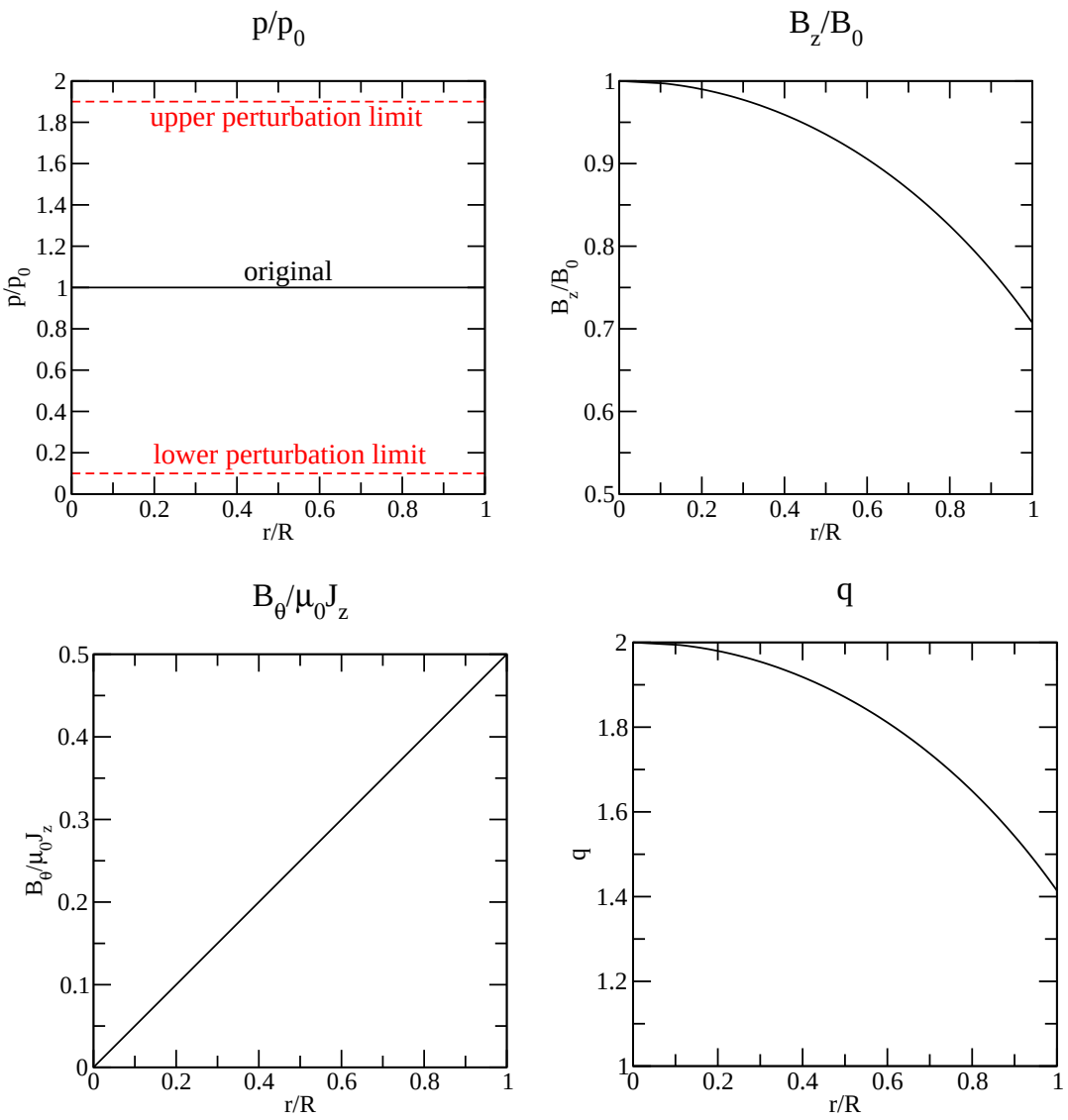

Figure 3.4: Initial and perturbed pressure, magnetic field and q profiles for screw pinch with constant pressure and constant current.

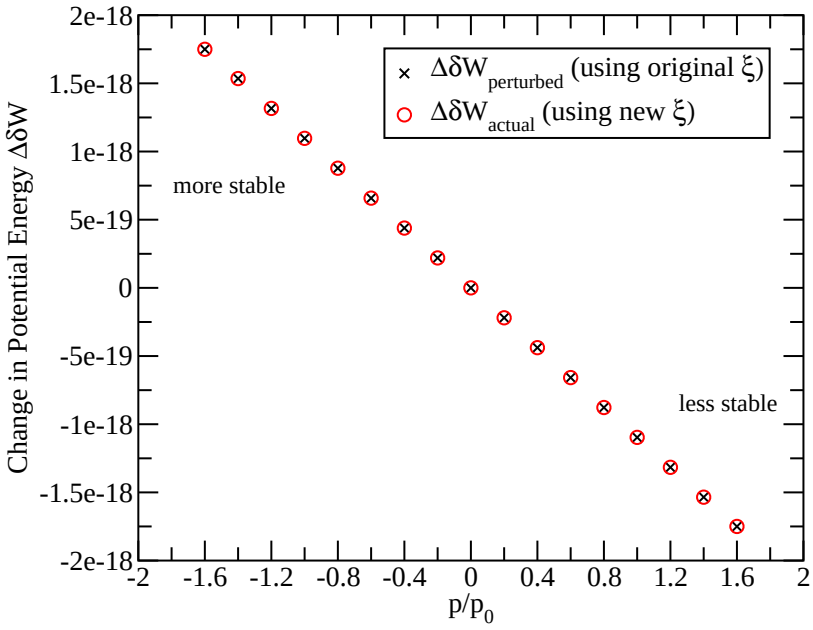

Figure 3.5: Perturbed and actual $\Delta\delta W$ for pressure variations of the screw pinch equilibrium with flat pressure and current profiles, for $k/m = 1/1$.

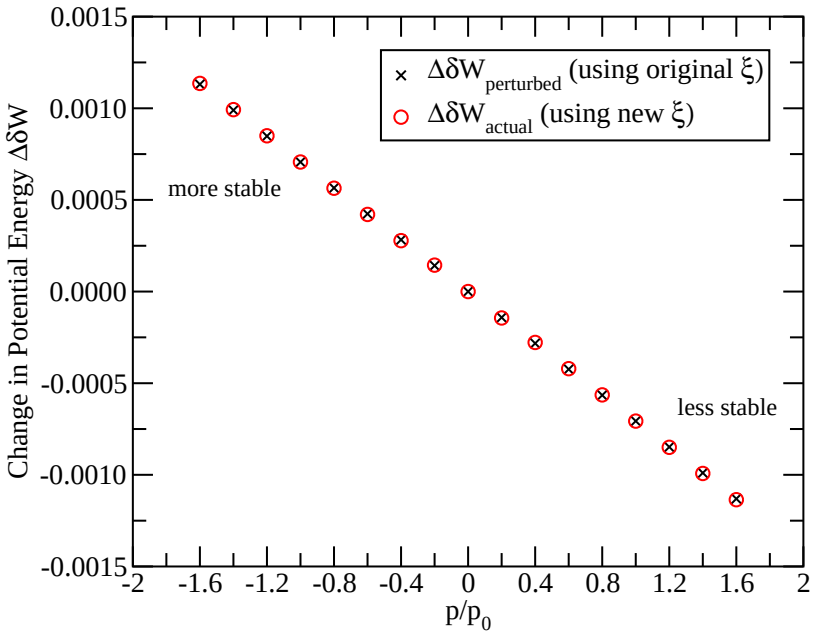

Figure 3.6: Perturbed and actual $\Delta\delta W$ for pressure variations of the screw pinch equilibrium with flat pressure and current profiles, for $k/m = 1/2$.

3.3 Perturbation of screw pinch equilibria with parabolic pressure and constant current profiles

For the next set of equilibria, the current profile remains flat ($J_z/J_0 = 1$), but the pressure profile is now more realistic: $(p/p_0 = 1 - (r/R_0)^{\alpha_3})$. Initially, $\alpha_3 = 2$, and is then perturbed from $\alpha_3 = 3/2$ to $\alpha_3 = 5/2$. The initial and perturbed profiles are shown in Figure 3.7.

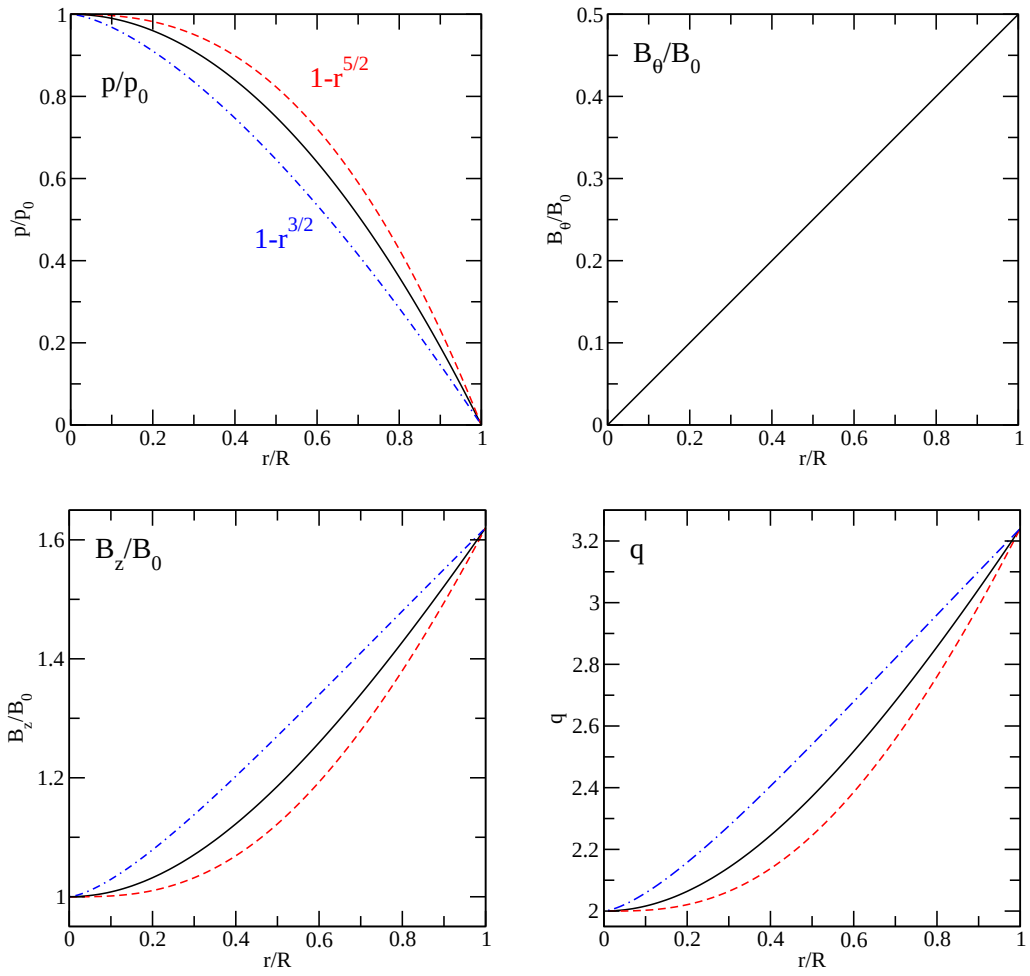

Figure 3.7: Initial and perturbed pressure, magnetic field, and q profiles for screw pinch with parabolic pressure and constant current.

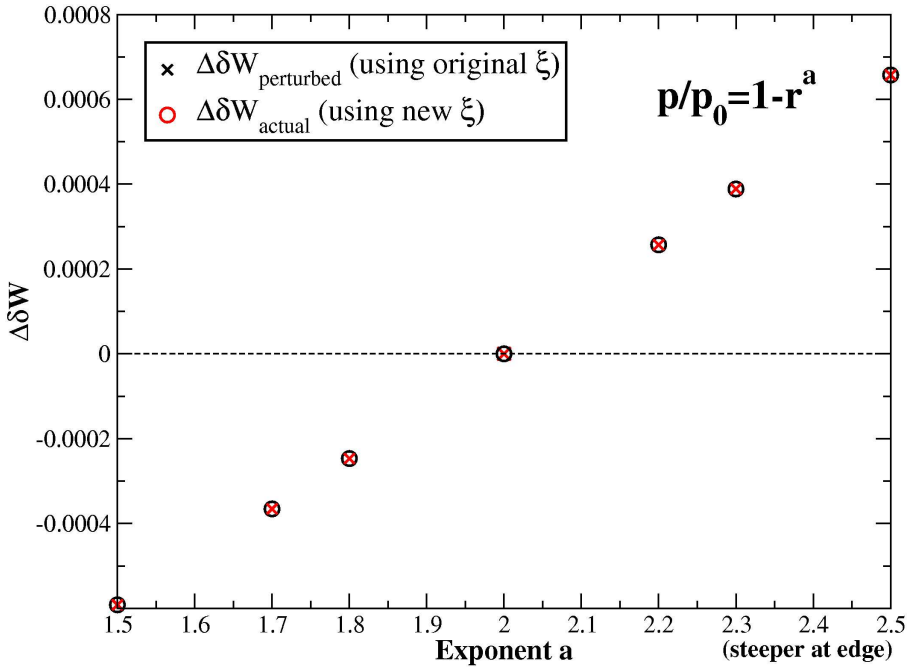

Figure 3.8: Perturbed and actual $\Delta\delta W$ for pressure variations of the screw pinch equilibrium with parabolic pressure and current profiles, for $k/m = 1/2$.

As before, $\underline{\xi}$ and δW are first found for the original equilibrium. Using the same $\underline{\xi}$, δW is then found for the perturbed equilibria. For comparison, the new $\underline{\xi}$ and corresponding δW are also found for each perturbed equilibrium. The perturbed and complete $\Delta\delta W$ calculations agree well over the range of perturbations, as shown in Figure 3.8 for $k/m = 1/2$.

Using $k/m = 1/1$ gives similar results. The displacements for $k/m = 1/1$ in Figure 3.9 show no discontinuity, as would be expected for an equilibrium with no $q = 1$ rational surface.

Also, the stability trend agrees with theory. A more steeply curved pressure profile (with constant J_z) increases the pressure-driven interchange component of $\Delta\delta W$:

$$\Delta\delta W_{pressure} = -2(\underline{\xi} \cdot \underline{\nabla} p)(\underline{\xi} \cdot \underline{\kappa}) \tag{3.17}$$

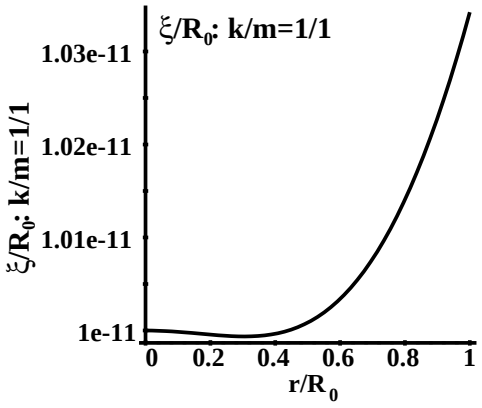

Figure 3.9: Displacements for $k/m = 1/1$ with parabolic pressure profile.

For positive ξ, the steeper profile ($\alpha_3 = 5/2$) gives $\Delta\delta W_{pressure} \sim 5r^{3/2}$, while the more linear profile ($\alpha_3 = 3/2$) gives $\Delta\delta W_{pressure} \sim 3r^{1/2}$. In addition, Figure 3.10 shows that the steeper profile has the highest increase in $\underline{\nabla} p$ where the displacements are highest.

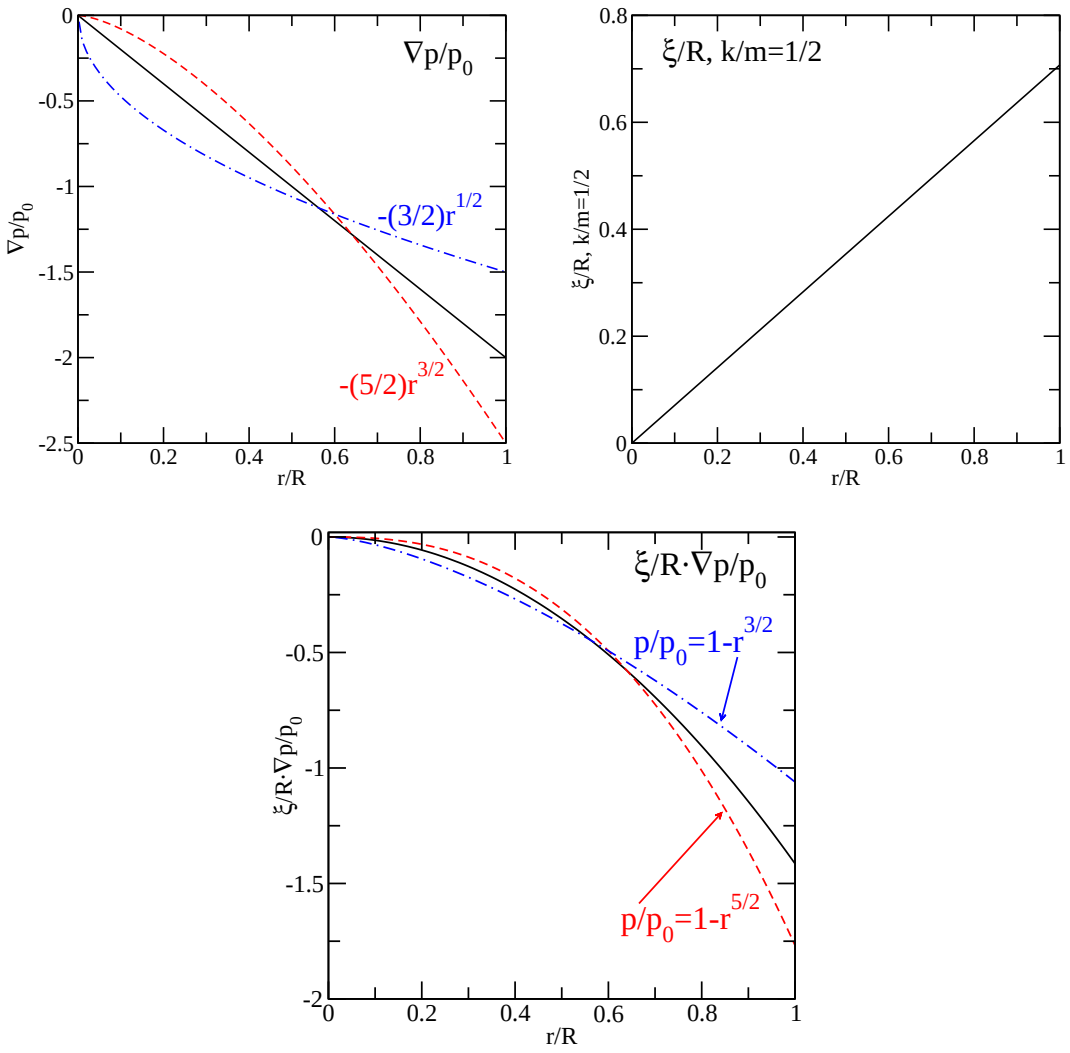

Figure 3.10: For the steeper profile ($p \sim 1 - r^{5/2}$), the pressure gradient increases most where the displacements are largest, which destabilizes $\Delta\delta W_{pressure}$.

3.4 Perturbation of screw pinch equilibria with constant pressure and stepped current profiles

For the next set of equilibria, the pressure profile remains flat ($p/p_0 = 1$). The current profile is piece-wise flat, but has a step at $r = R_{step}$:

$$J_z(r) = \begin{cases} J_0 & (r < R_{step}), \\ \alpha_5 J_0 & (r > R_{step}). \end{cases} \tag{3.18}$$

The current is initially flat, and the step height is perturbed from $\alpha_5 = 0$ to $\alpha_5 = 2$ at $R_{step} = 0.5$. The current and q profiles are shown in Figure 3.11.

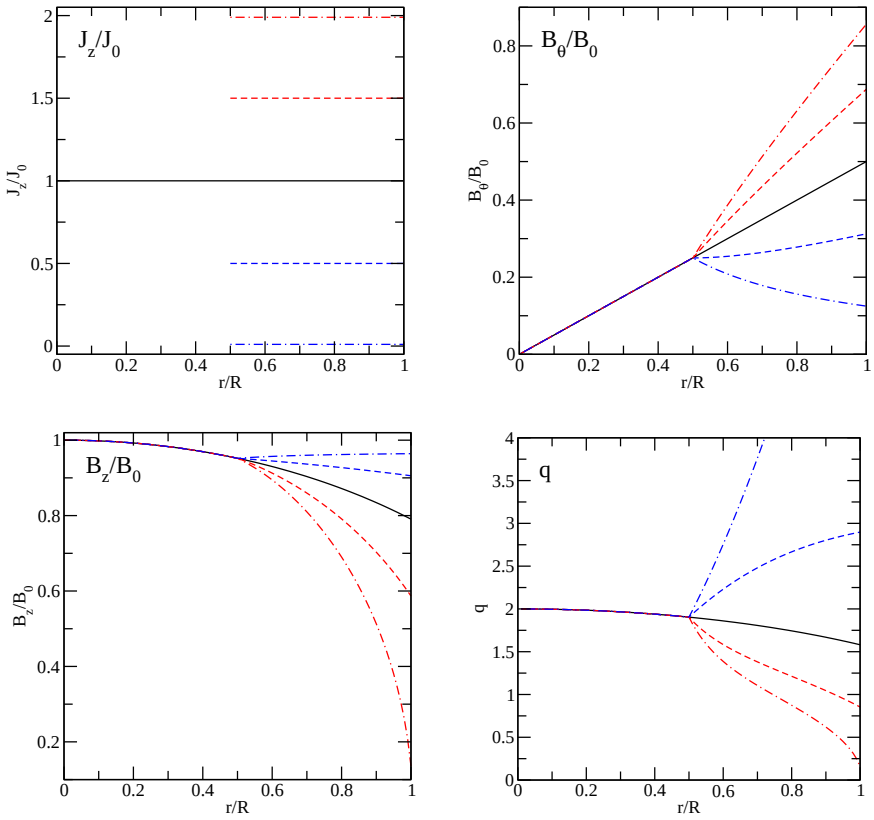

Figure 3.11: Initial and perturbed current, magnetic field and q profiles for screw pinch with constant pressure and stepped current.

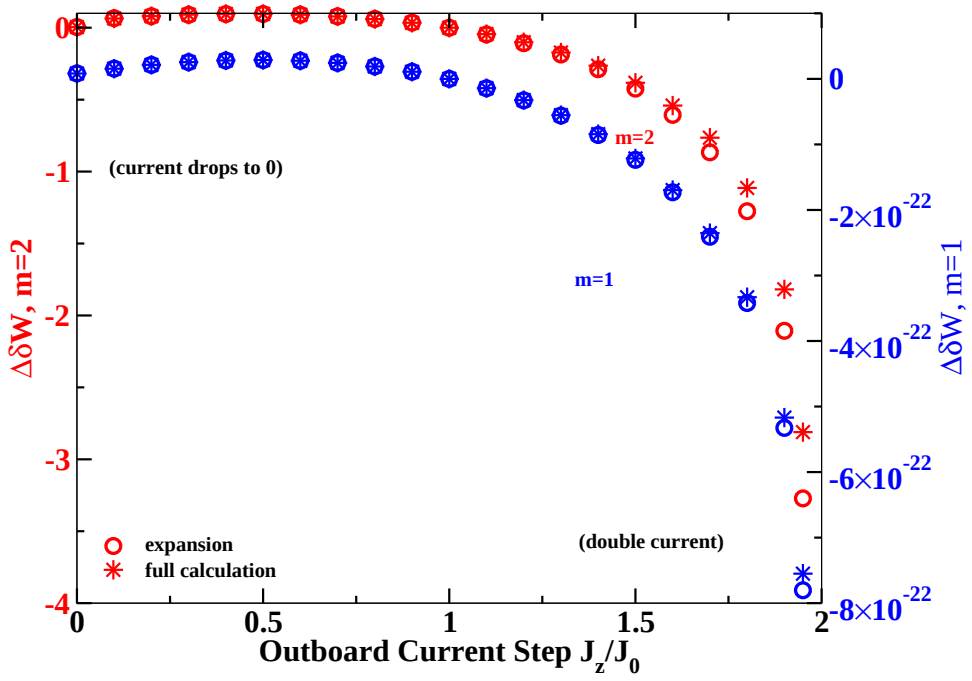

Figure 3.12: Perturbed and actual $\Delta\delta W$ for current step height variations of the screw pinch equilibrium with flat pressure and stepped current profiles, for $k/m = 1/2$ and $k/m = 1/2$.

As before, both the original and new displacements are computed, and $\Delta\delta W$ found using each. Figure 3.12 shows good agreement between perturbed (computed with original ξ) and actual $\Delta\delta W$(computed with new ξ) for both $k/m = 1/1$ and $k/m = 1/2$. The agreement is not as good when the stepped current doubles ($\alpha_5 = 2$), but the trend is still correct. Results are similar when the pressure profile is parabolic rather than flat.

Stability degrades as the outboard current step is increased, which agrees with analytic theory. The current-driven kink mode is proportional to J_z:

$$\delta W_{current\ driven\ kink} = \frac{\underline{J} \cdot \underline{B_0}}{|B_0|^2} \underline{B_0} \times \underline{\xi} \cdot \underline{B}. \tag{3.19}$$

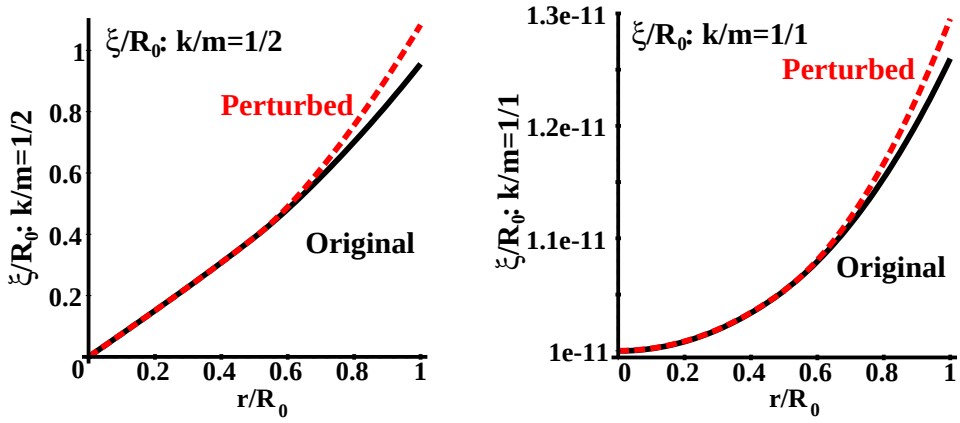

Figure 3.13: Displacements for initial flat current and perturbed current with outboard current step $J_z/J_0 = 0.1$.

The initial displacements are very close to the actual displacements for the perturbed equilibria. When J_z approaches zero in the outboard step, displacements for the original and perturbed equilibria differ by about 10% at the edge for both $k/m = 1/1$ and $k/m = 1/2$, as shown in Figure 3.13. This is also the region where $\Delta\delta W$ comparisons deteriorate.

3.5 Perturbation of screw pinch equilibria with curved pressure and current profiles

The final set of screw pinch equilibria have both parabolic pressure and current profiles: $p/p_0 = 1 - (r/R_0)^{\alpha_3}$ and $J_z/J_0 = 1 - (r/R_0)^{\alpha_1}$. These equilibria have low q in the center and high magnetic shear (gradient of q) toward the edge. By changing B_z on axis while fixing pressure and current profiles, we vary q in the center from $q_{axis} = 0.5$ to $q_{axis} = 1.0$, leaving q_{edge} fixed. Pressure and q profiles are shown in 3.14.

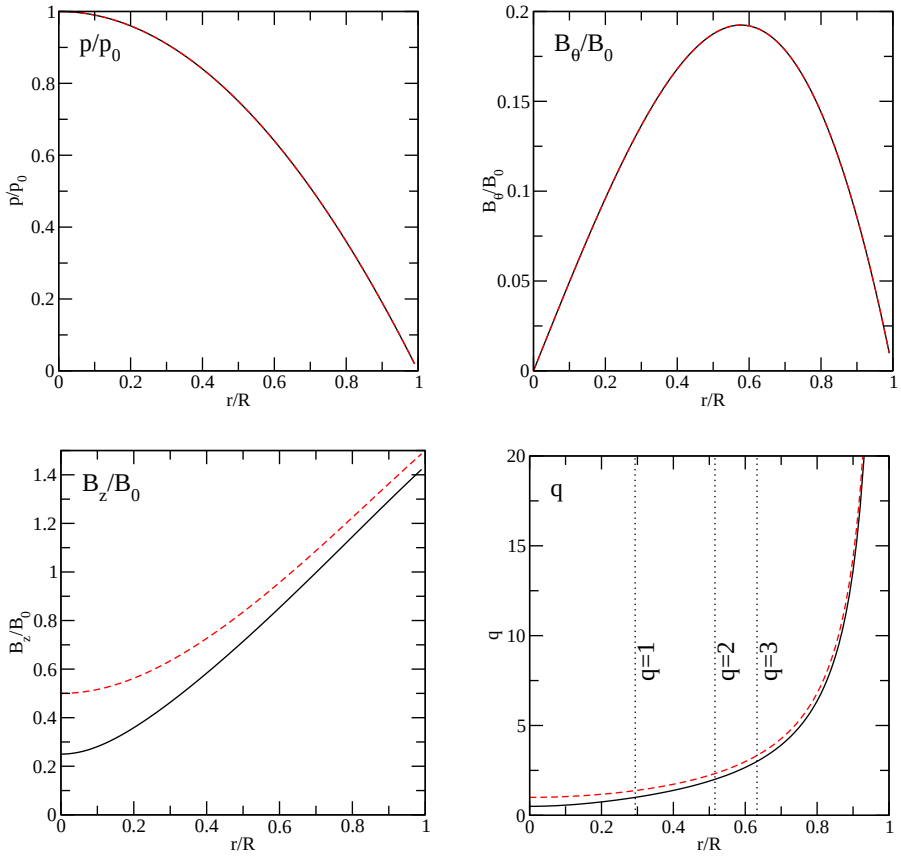

Figure 3.14: Initial and perturbed pressure, magnetic field and q profiles for screw pinch with parabolic pressure and current.

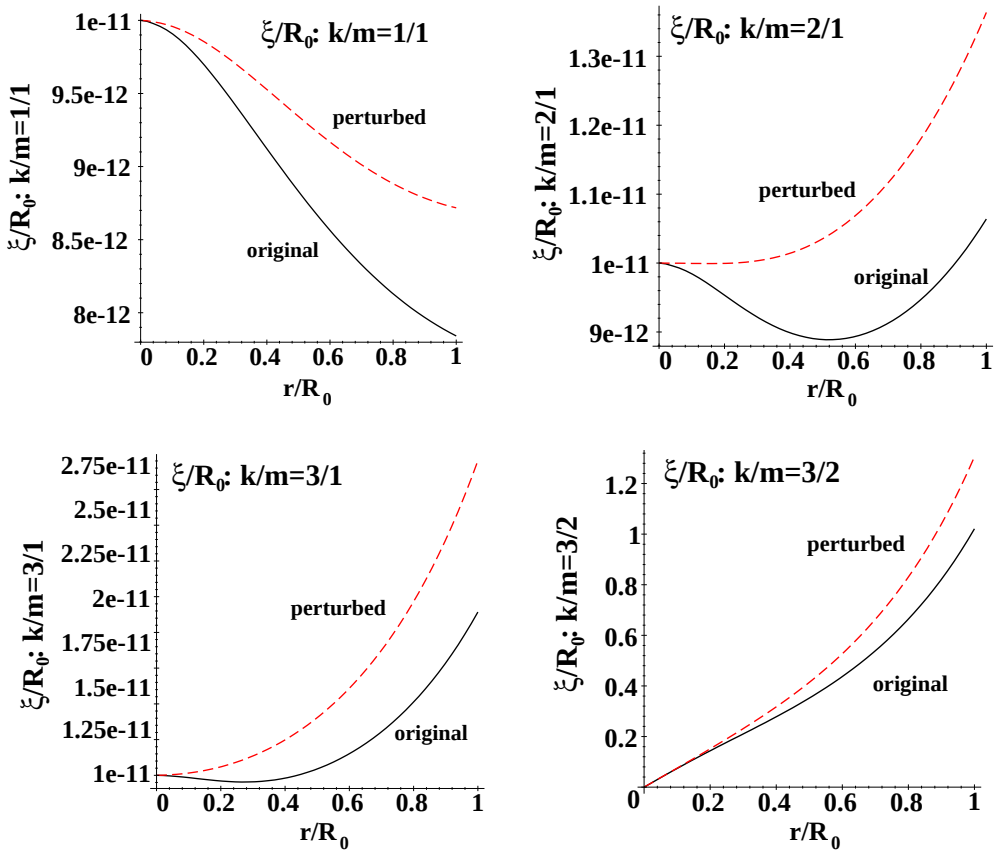

Figure 3.15: Displacements for several k/m for screw pinch equilibria with parabolic current and pressure profiles. Raising q_{axis} from 0.5 to 1 increases ξ for all the k/m examined.

Figure 3.15 displays displacements for both the initial and perturbed equilibria, for $k/m = 1/1, 2/1, 3/1$, and $3/2$. In all cases, displacements are global and the greatest deviation in ξ near the edge is 20% - 30%.

These equilibrium profiles push the limits of semi-analytic treatment. While ξ can be found, solving for δW requires more sophisticated techniques. Qualitatively, raising q_{axis} from 0.5 to 1 increases δW inside the surface where $q = k/m$ (as expected for stabilization of internal kink), as shown in Figure 3.16 for $k/m = 1/1$. However, the accompanying increased ξ outside the $q = k/m$ surface decreases δW and the total

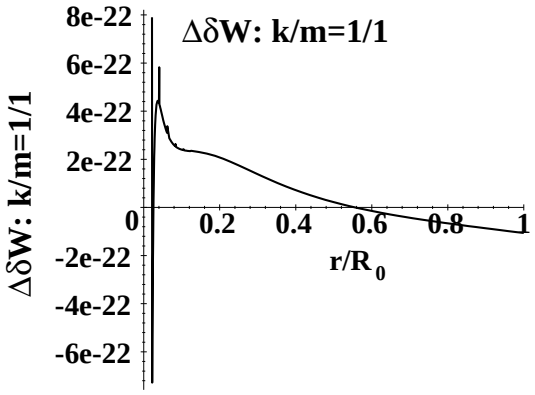

Figure 3.16: $\Delta\delta W$ for q_{axis} perturbations of screw pinch equilibria with parabolic current and pressure profiles, for $k/m = 1/1$. Increasing q_{axis} from 0.5 to 1 increases $\Delta\delta W$ inside the $q = k/m$ surface, but decreases $\Delta\delta W$ everywhere else.

$\Delta\delta W$ is negative (external kink) for all the k/m modes examined.

Compared to the change in displacements associated with perturbing other screw pinch equilibria, $\Delta\xi$ here is relatively large at the edge. However, $\Delta\xi$ is still smooth with no large or abrupt changes at the $q = k/m$ surface. Also, $\Delta\xi$ is usually still small over most of the plasma. Because only small regions of the plasma are affected and $\Delta\xi$ is well-behaved, perturbing q in toroidal equilibria is not expected to be problematic. However, because $\Delta\xi$ is largest here, q perturbations may be the most limited.

3.6 Positive results from perturbing the screw pinch

Perturbing screw pinch equilibria to obtain $\Delta\delta W$ works well, and no major obstacles were discovered. The exploration found that:

- For flat pressure and current profiles, the stability is correctly predicted over the entire wide range of pressure perturbations ($p/p_0 = 0.1$ to 2.0).

- For curved pressure and flat current profiles, the stability is correctly predicted

when the pressure profile is made steeper or shallower ($p/p_0 = 1-(r/R_0)^{\alpha_3}, \alpha_3 =$ 3/2 to 5/2).

- For stepped current profiles with either curved or flat pressure profiles, the stability trends are correct over a wide range of step heights.

- For curved pressure and current profiles that exhibit high edge shear and contain $q = 1$ surfaces, displacements are not as inconsistent between the original and perturbed equilibria as initially suspected. Only small regions of the plasma are affected. However, these situations may still limit the technique.

Because this analysis used a form of the Lagrangian that eliminated compressional Alfvén energy, it is not a complete test of our perturbative method. Including the compressional Alfvén energy, however, would have introduced singular surfaces and required a more computational (rather than analytic) treatment of the screw pinch. Although this might have revealed difficulties with the compressional Alfvén term, as will be seen in the toroidal application, it would not have been immediately clear that neither the method itself nor the presence $q = 1$ surfaces caused poor results.

Chapter 4

Toroidal Perturbations

Encouraged by the results of perturbing δW for the screw pinch, we progressed to perturbing experimental toroidal equilibria. While the perturbation technique is general enough to be used with any source of equilibria and any MHD stability code that produces a displacement vector, we used EFIT [14] to generate experimental equilibria and GATO [3] for stability results. We also used TOQ [16, 17] later to generate simplified equilibria. This chapter will first describe features of GATO, then present results for perturbing experimental and simplified equilibria. In general, perturbing wall parameters worked quite well, but perturbing plasma parameters beyond a very small range resulted in large errors in $\delta W_{perturbed}$.

4.1 Features of GATO

The stability code GATO computes ideal MHD mode frequencies and displacements by minimizing δW in the energy principle (Equation 2.1). The problem is recast as a matrix eigenvalue problem:

$$AX = \gamma BX, \tag{4.1}$$

where the matrices A and B represent the potential and kinetic energy matrices, X is the displacement vector represented by finite hybrid elements (discussed in Chapter 2), and the eigenvalue $\gamma = \omega^2$ is the mode growth rate. If $\gamma > 0$ then ω is real and the

equilibrium is stable. If any $\gamma < 0$ then ω is imaginary and the system is unstable.

GATO consists of four modules; some have been re-used or modified for the perturbed stability calculation:

- Mapping: The equilibrium data is first mapped from the equilibrium mesh (which may be in (r, z) coordinates) to the flux coordinate mesh that GATO uses. GATO's mesh is generally optimized so there are more computational surfaces packed near integral values of q. To eliminate errors arising from changes in the basis functions used to generate the finite elements, the perturbed stability calculations use the same flux surface packing and computational mesh as the original stability calculation. GATO's coordinates, designed for computational efficiency, were described in Chapter 2. They are reiterated here:

$$\begin{aligned} X &= J|\nabla\psi|\xi_s/r^2, \\ U &= 2s\psi_s\xi_\chi/r|\nabla\psi| - Y + \beta_\chi X, \\ Y &= 2s\psi_s\xi_\phi/I_p r, \end{aligned} \tag{4.2}$$

- Vacuum and energy matrices: Next GATO defines the wall from input parameters, determines the vacuum contribution, and constructs the potential and kinetic energy matrices A and B. This module is repeated in the perturbed stability calculation.

- Eigenvalue solver: Solving the eigenvalue equation is very computationally intensive. For the perturbed stability calculations, this module is replaced by the simple matrix multiplications $A_{perturbed}X_{original}$ and $B_{perturbed}X_{original}$ to obtain the perturbed δW and K.

- Output analysis: Finally, GATO output is created. Output is highly customizable, and may include energy contributions, Fourier decompositions, and various components of $\underline{\xi}$ and the perturbed magnetic field $\delta\underline{B}$, all as plots or data files. Any of several coordinate system may be chosen for $\underline{\xi}$ and $\delta\underline{B}$ representation: GATO's coordinate system, field line coordinates, cylindrical coordinates, or normal orthogonal coordinates.

In the previous chapter, results for the screw pinch were presented as $\Delta\delta W$. For toroidal results, computational accuracy and rounding error issues suggest presenting comparisons of δW_{actual} and $\delta W_{perturbed}$ instead. Comparisons also reveal whether, for example, a small $\Delta\delta W$ reflects a very small difference between two large numbers, or a measurable difference between two numbers of the same (small) order of magnitude.

4.2 Benefits beyond routine GATO computations

In addition to quickly estimating stability trends, our method yields more information than might be readily obtained with routine GATO runs. Conditions corresponding to marginal stability are more quickly determined. Also, full GATO computations that have inherent (but unforeseeable) convergence problems may be avoided with our method.

Determining conditions corresponding to marginal stability is generally tedious. Stabilty codes such as GATO are designed to find an unstable mode, and the run time can easily double the if the mode is truly stable. After a lengthy computation, the code may abort with an error that may or may not indicate a stable mode. The perturbed δW method simply multiplies matrices, whether the eigenvalue is stable or unstable. This allows parameters corresponding to marginal stability to be quickly determined.

Occasionally full GATO computations have difficulty converging on an eigenvalue. Convergence issues cannot be entirely predicted before starting a computation, but may be side-stepped with our perturbative method. With certain equilibria and input options, GATO may not converge on the eigenvalue (changing input options or the mesh usually solves this problem). The matrix multiplication at the heart of our perturbation technique does not have the convergence issues associated with iteration, and can be used to avoid possible unconverged GATO computations. More accurate results may be desired for a perturbed run, an investigator can not know beforehand if a full GATO calculation will have difficulty converging. Results from $\delta W_{perturbed}$ can be used as an initial guess to the eigenvalue problem, decreasing GATO's computation time and improving chances for convergence.

4.3 Perturbations of wall parameters with experimental equilibria

For perturbations of wall parameters with experimental toroidal equilibria, we began with DIII-D discharge 92691. Pressure and q profiles for 92691 are shown in Figure 4.1. Two initial walls, shown in Figure 4.2, were perturbed:

- a conformal wall extended a constant distance D from the plasma surface, and
- a symmetric parameterized D-shaped wall, in roughly the same location as the conformal wall.

Note that neither of these walls represents the actual wall of DIII-D, which stabilizes the $n = 0$ mode. Conformal walls are commonly used in MHD studies to easily assess general wall effects.

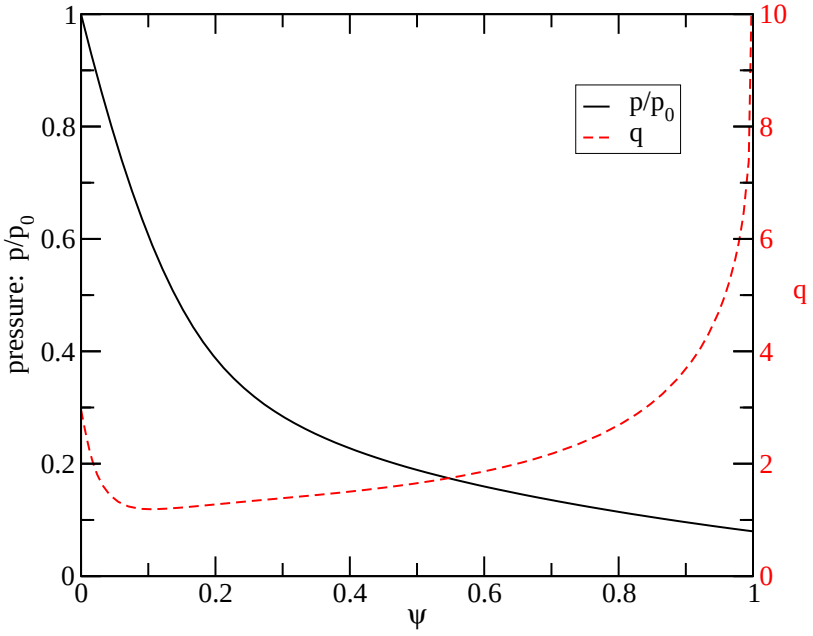

Figure 4.1: Pressure and q profiles for DIII-D discharge 92691.

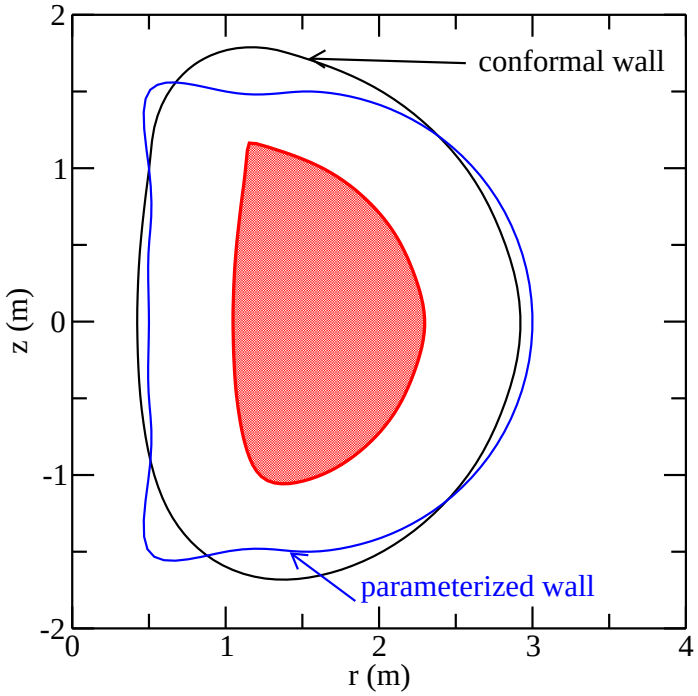

Figure 4.2: Unperturbed conformal and parametrized walls.

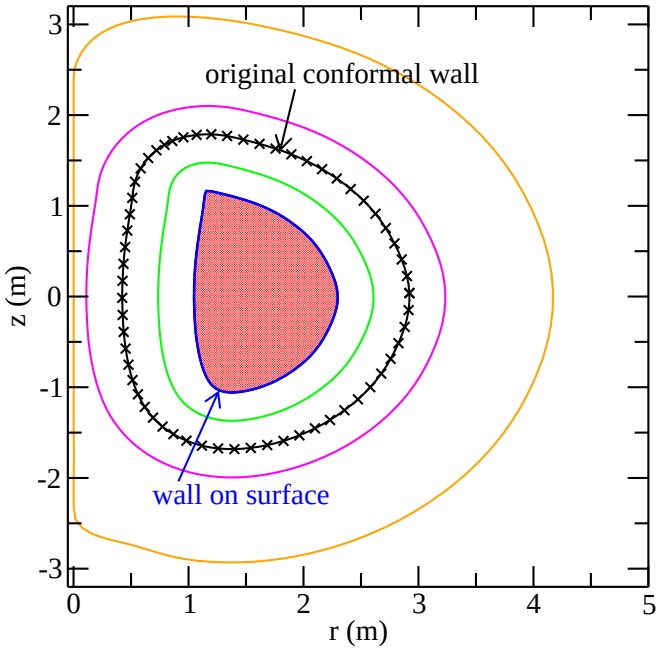

Figure 4.3: Conformal wall perturbations about the initial wall position at distance D / minor radius $r = 1$

The parameterized wall was constructed to enable systematic variations in location and shape of various segments of the wall. Similar wall perturbations may:

- determine the optimum wall distance needed to stabilize a particular mode,
- assess the impact of a smaller central hole in the torus or additional hardware,
- investigate performance of novel wall shapes, and
- test new divertor designs or liquid wall components.

For the conformal wall perturbations, the wall distance was varied from the closest non-stable wall distance to infinity (no wall), illustrated in Figure 4.3. Perturbations of this kind allow an investigator to determine the wall distance needed to stabilize a particular mode. Figures 4.4 and 4.5 show very good agreement between $\delta W_{perturbed}$ and δW_{actual} for both $n = 1$ and $n = 0$ over the entire range of wall positions. Nothing

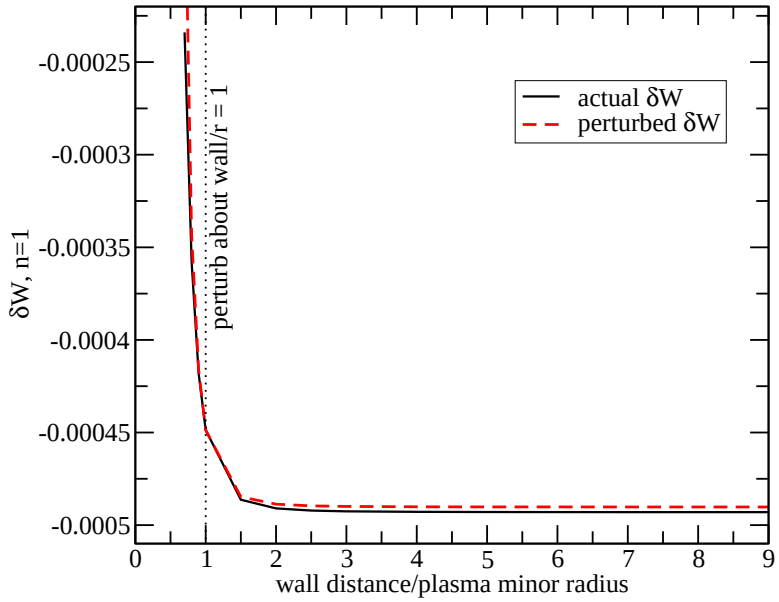

Figure 4.4: Perturbed and actual δW for $n = 1$ agree over a wide range of conformal wall distance perturbations.

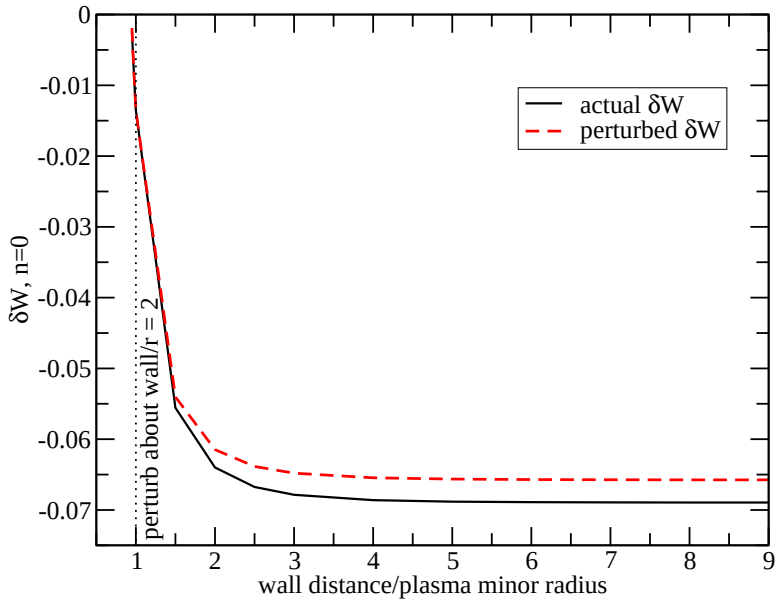

Figure 4.5: Perturbed and actual δW for $n = 0$ agree over a wide range of conformal wall distance perturbations.

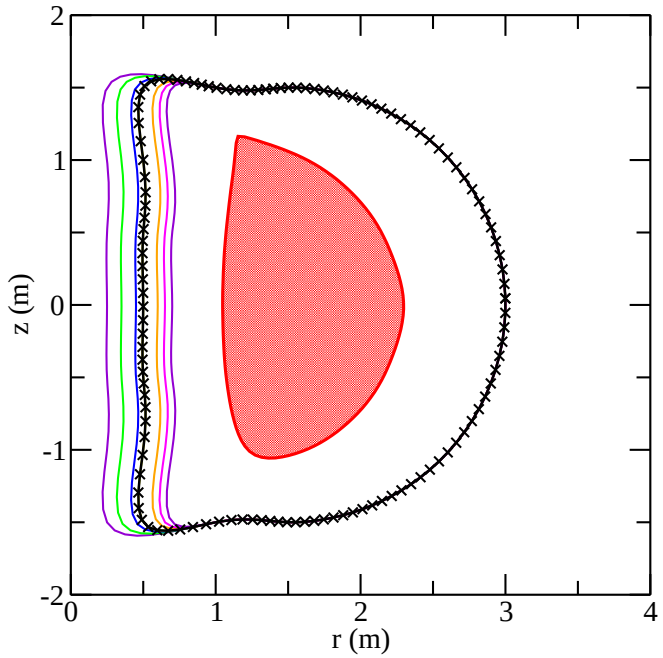

Figure 4.6: Inboard wall distance spacing varied from a distance $D = 0.28w$ to $0.64w$, about $D = 0.44w$ (w = plasma width measured at the midplane).

about the equilibrium plasma was varied; only the vacuum energy changed in the stability calculation. The only deviation of $\underline{\xi}_{actual}$ from $\underline{\xi}_{original}$ occurs on the very last computational surface — the very edge of the plasma. The bulk of the stability calculation is identical for all wall positions.

With both $n = 1$ and $n = 0$, $\delta W_{perturbed}$ at no wall did not appreciably change from $\delta W_{perturbed}$ at $D \approx 5r$. Although $\delta W_{perturbed}$ is estimated slightly higher than δW_{actual} for the greater wall distances, the trend and close distance details are correct.

Conformal walls offer no other meaningful perturbations, so we now turn to the parameterized wall. The spacing between the inboard segment of the parameterized wall and the inboard plasma surface was varied first, perturbing about a distance $D = 0.44w$ (w = plasma width measured at the midplane), from $D = 0.28w$ to $0.64w$. The perturbations are illustrated in Figure 4.6. These kinds of perturbations might

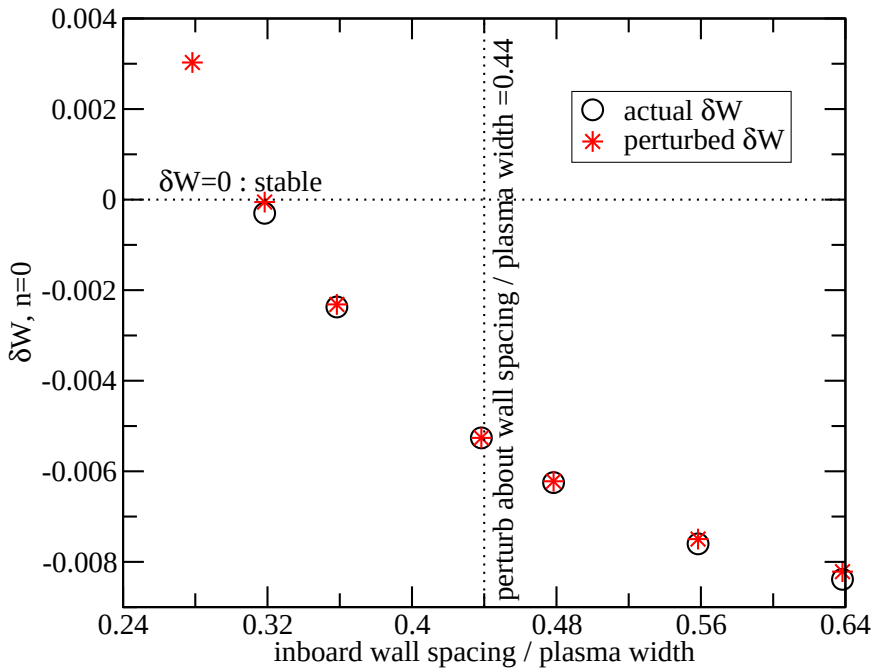

Figure 4.7: Perturbed and actual δW for $n = 0$ have excellent agreement for inboard plasma-wall spacing perturbations with the parameterized wall.

allow an investigator to assess the impact of additional inboard hardware, or of a smaller central hole in the torus. For $n = 0$, $\delta W_{perturbed}$ and δW_{actual} agreed over the range of unstable δW examined, as illustrated in Figure 4.7. With the wall closer than $D = 0.32w$, the $n = 0$ mode was stabilized. Because GATO does not normally report stable eigenvalues when it is searching for unstable modes, there are no δW_{actual} results from GATO for comparison.

Remaining on the inboard side, the flat section of the parameterized wall was varied next, and $\delta W_{perturbed}$ calculated for $n = 0$. The inboard wall was given up to four sinusoidal periods, as shown in Figure 4.8. Each sinusoidal wall is centered on the original parameterized wall, and all have the same top, bottom, inboard corners, and outboard wall positions. These variations of the inboard wall shapes are on the path

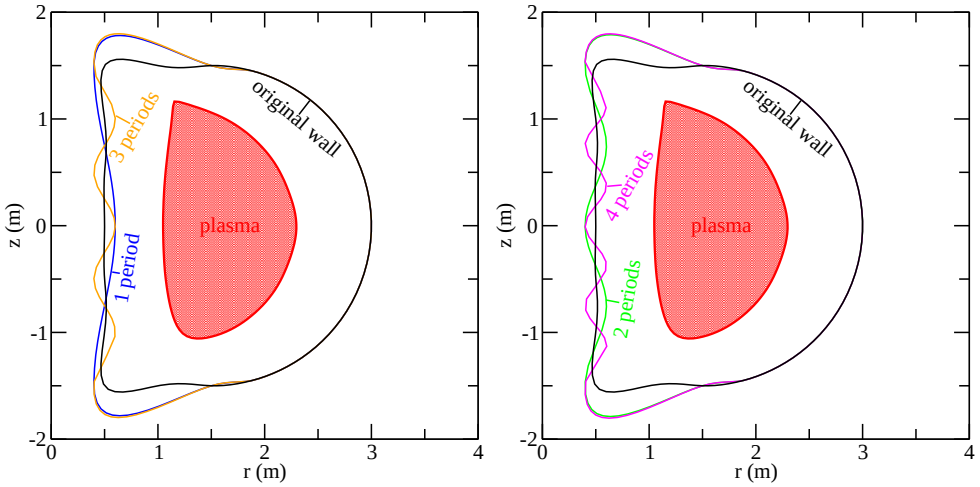

Figure 4.8: Sinusoidal inboard wall perturbations have central sections of the wall closer to plasma when there are an odd number of sinusoids.

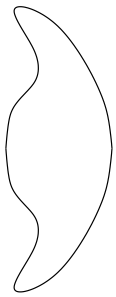

Figure 4.9: A novel torus cross section has been proposed to increase plasma stability to $n = 0$ mode.

to investigating a new wall shape, shown in Figure 4.9, that might better stabilize $n = 0$ modes. Candidate equilibria are still being developed by other researchers for investigating this shape.

With an odd number of periods (1,3), the center sinusoid moves the wall closer to the plasma at the midplane, while walls with an even number (2,4) move the central section farther away. Based on the results from moving the entire inboard wall closer to or farther from the plasma, we should see the walls with odd numbers of periods stabilize the $n = 0$ mode most.

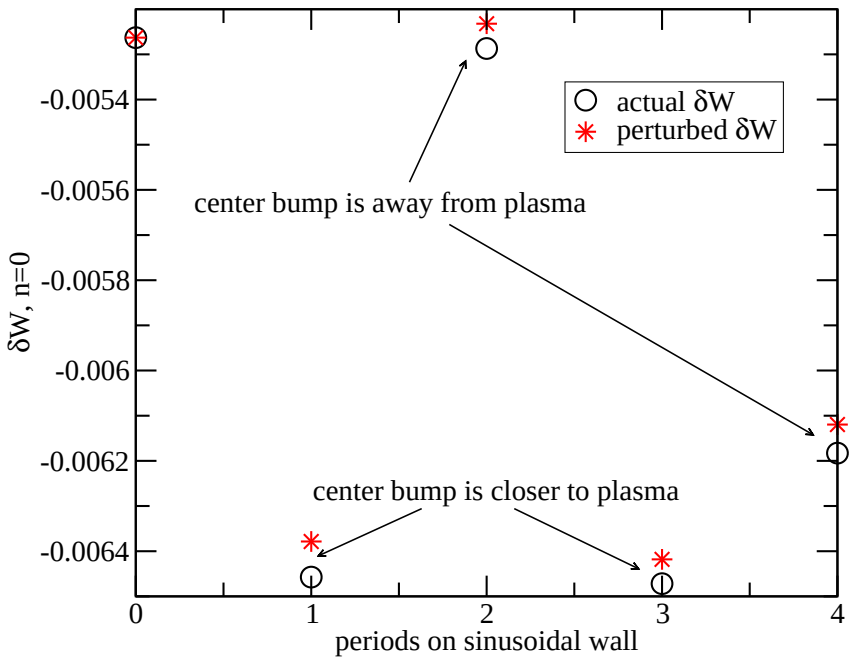

Figure 4.10: Perturbed and actual δW for $n = 0$ agree when the sinusoidal inboard wall shape is perturbed.

Figure 4.10 compares $\delta W_{perturbed}$ and δW_{actual}, perturbing from the original parameterized wall. As expected, stability is sensitive to whether the central sinusoid is closer to or farther from the plasma, but only for walls with few periods. The 4-period wall is almost as stabilizing as the walls with 1 or 3 periods, while the 2-period wall is only slightly different from the original flat wall. More periods also appear to be more stabilizing, although in this example the wall distance is probably a bigger factor.

Similar to results from moving the conformal wall, $\delta W_{perturbed}$ and δW_{actual} do not agree exactly, but they have the same general response. The agreement would likely improve if the inboard corners for the sinusoidal walls and the original wall were at the same location.

Next, the top and bottom distance of the parameterized wall was varied, illustrated in Figure 4.11, and again for $n = 0$. Similar perturbations might be used to assess

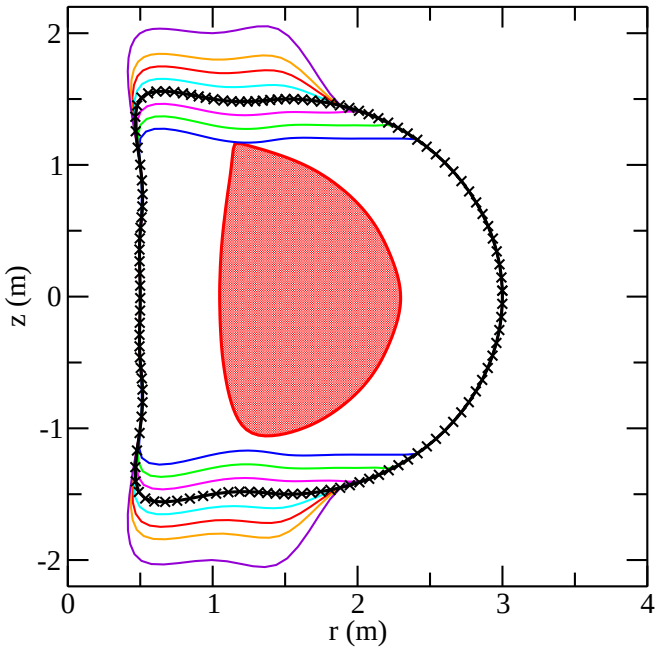

Figure 4.11: Wall top and bottom distances varied while leaving inboard and outboard wall position and shapes unchanged.

new divertor designs, liquid wall components, or other hardware. Because the $n = 0$ mode produces a vertical plasma displacement, changing wall height is expected to have a greater effect than changing the inboard or outboard wall. With this particular equilibrium from 92691, Figure 4.12 shows that the wall height can only be slightly decreased from the original parameterized wall before the $n = 0$ mode is stabilized. Compared to moving the inboard wall, where $\delta W_{perturbed}$ was only on the order of 10^{-3}, changing wall height does effect the stability more, with δW on the order of 10^{-2}.

The perturbation technique also gives several results for wall heights that stabilize the $n = 0$ mode, which GATO did not produce. Codes such as GATO try very hard to find an unstable mode, which can easily double the run time if the mode is truly stable. Furthermore, after spending so much computation time, GATO aborts with an error that may or may not indicate a stable mode. Because the perturbed δW method

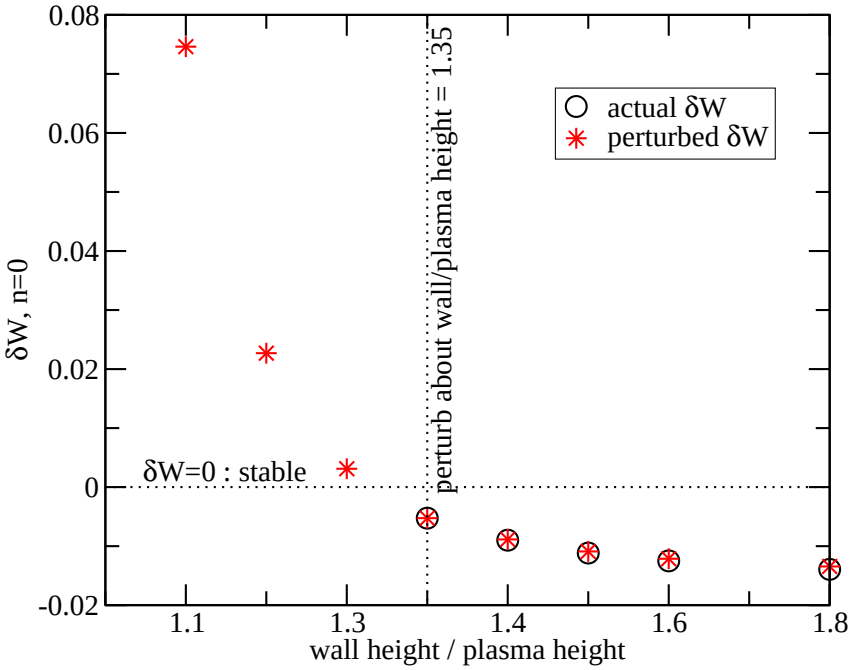

Figure 4.12: For δW unstable to $n = 0$, perturbed and actual δW agree when parameterized wall height is perturbed.

doesn't know about stable eigenvalues but rather simply multiplies matrices, it can be used to quickly locate wall parameters corresponding to marginal stability.

Finally, the location of the outboard wall was varied, again for $n = 0$. As shown in Figure 4.13, the general curve of the outer wall did not change, but the D shape became wider or narrower. Figure 4.14 compares only four instances of δW_{actual} with $\delta W_{perturbed}$: one at the perturbation center, two nearby, and one with a large wall distance. With the outboard wall closer than a distance $D = 0.6w$, the $n = 0$ mode is stabilized, so there are no δW_{actual} results to compare at these closer distances. Numerical convergence issues also resulted in the wrong δW_{actual} values[1] for most intermediate wall distances.

[1]We know these values are wrong from convergence results reported by GATO, and also because they are positive. Positive results from GATO are possible, but not with the input parameters given for these calculations.

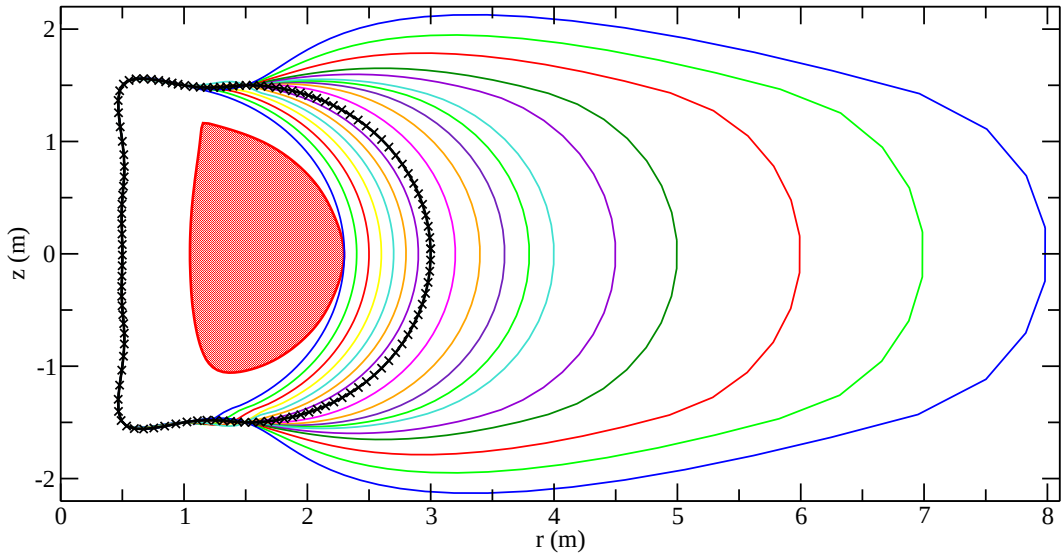

Figure 4.13: Outer wall distance was varied without changing the inboard wall.

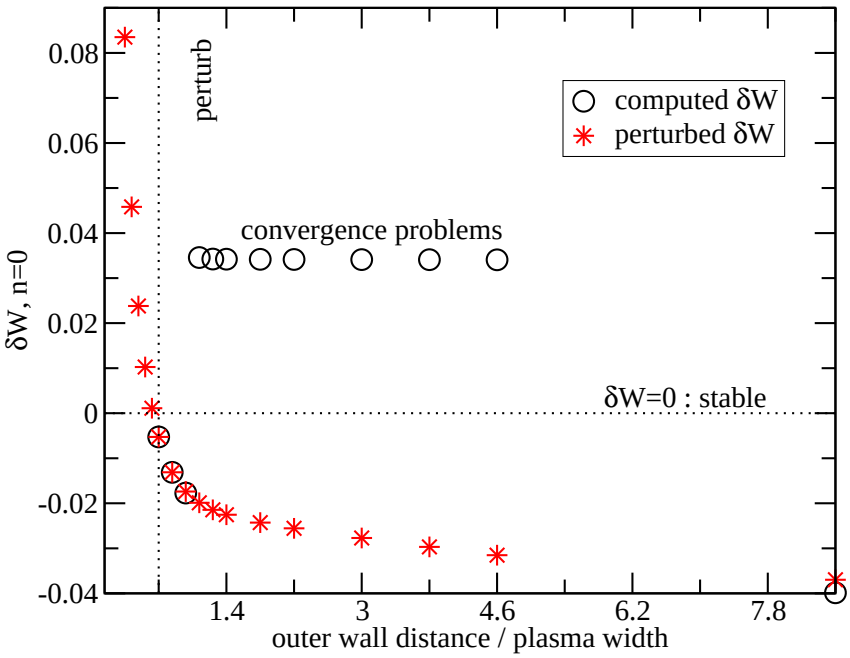

Figure 4.14: Perturbed and actual δW for perturbations to the outboard segment of parameterized wall agree where actual results are available.

In some situations, GATO may try to converge on an eigenvalue in the wrong direction (changing input parameters or the mesh usually solves this problem). The perturbation technique doesn't have convergence issues with simple matrix multiplication, and can be used to avoid possible unconverged GATO runs. An investigator may want more accurate results for a perturbed run, but does not know beforehand if a GATO calculation will have difficulty converging. Results from $\delta W_{perturbed}$ can be used as an initial guess to the eigenvalue problem, decreasing GATO's computation time and improving chances for convergence.

4.4 Perturbations of experimental equilibria

To test the perturbation technique with toroidal experimental equilibria, rather than with walls, we chose DIII-D discharge 87009 as the baseline equilibrium. This is a well-diagnosed shot, and the subject of several studies [39, 40, 41]. Figure 4.15 shows the q and pressure profiles. The q profile is relatively flat over most of the plasma, starting at $q_{axis} = 2.0498$. The profile dips below $q = 2.0$ briefly, and rises steeply

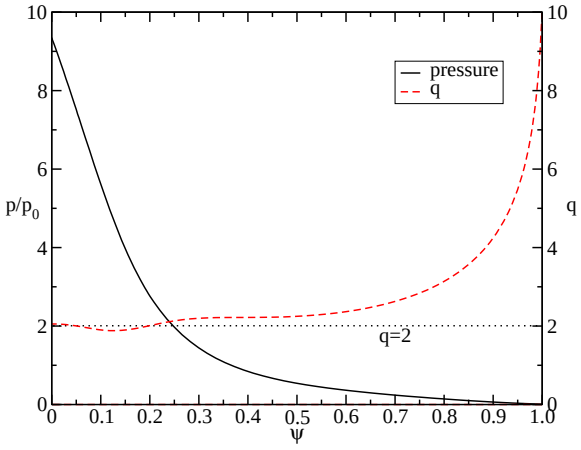

Figure 4.15: Pressure and q profiles for DIII-D discharge 87009.

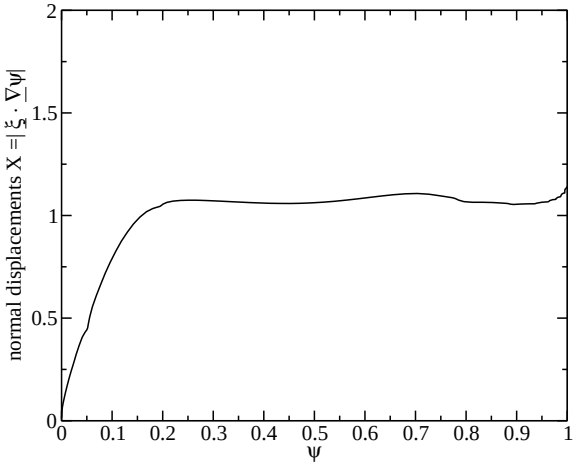

Figure 4.16: Normal $n = 1$ displacements for unperturbed DIII-D discharge 87009.

towards the edge.

Results from GATO indicate a global $n = 1$, $m = 3$ kink mode. There is also a $m = 2$ mode that increases displacements at the $q = 2$ surface. Figure 4.16 shows global normal displacements $X = \underline{\xi} \cdot \underline{\nabla}\psi$. As with most of the screw pinch equilibria, displacements do not abruptly change, although they increase steeply (but smoothly) for $\psi <\sim 0.2$

We perturbed the experimental equilibrium by scaling q. Input parameters to GATO allow scaling of the q profile by changing q_{axis} or q_{edge}, without generating a new equilibrium for each new q profile. Changing q in this way also similarly changes the equilibrium magnetic field. The pressure profile is not affected. Using GATO's input parameters, we perturbed about $q_{axis} = 2.0498$, from $q = 2.0$ to 2.1. These limits of perturbation, shown in Figure 4.17, were chosen to retain the dual $q = 2$ surfaces. Setting $q_{axis} > 2.1$ would miss $q = 2.0$ at the bottom of the dip. Allowing q_{axis} to drop below 2.0 would move the dip low enough to eliminate the first $q = 2$ surface.

As with the screw pinch, both actual and perturbed stability results were computed

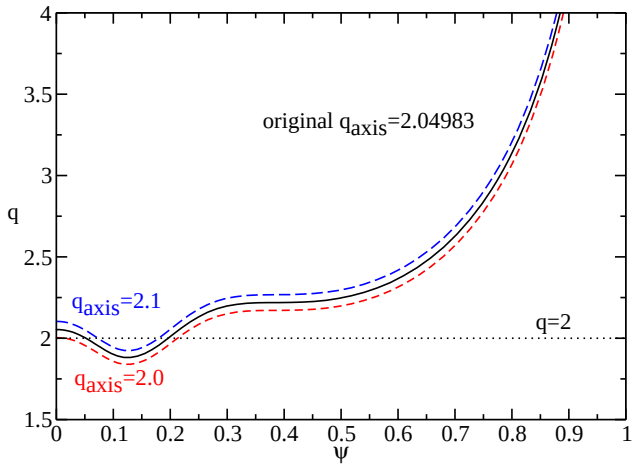

Figure 4.17: Limits of q-profile perturbation for DIII-D discharge 87009.

for comparison. All computations used the same computational grid and mapping, on a 100×200 $(\psi \times \chi)$ mesh. Results were quite different than those from the screw pinch. Figure 4.18 shows that very small changes to q_{axis} have a large effect on δW. For example, changing q_{axis} by only ~ 0.03 ($\sim 1\%$ change) increases δW by $\sim 50\%$. The perturbation results rapidly depart from the actual GATO results and agree only for extremely small perturbations.

A similar quadratic curve results from perturbing q_{edge}. The error consistently always increases, rather than under-estimating when perturbing in one direction and over-estimating when perturbing in the other. A parabolic curve on an energy plot usually immediately suggests a stable state at the energy minimum. In this case, the minimum of *perturbed* δW at $q_{axis} = 2.0498$ does not mean that the plasma is most stable there. This would be a valid interpretation only if the *actual* δW had a minimum at $q_{axis} = 2.0498$ as well.

The minimum instead comes about from re-using $X_{original}$. Recall that $\underline{\xi}$ is found by minimizing δW in the energy principle. If the wrong $\underline{\xi}$ is used to calculate $\delta W_{perturbed}$,

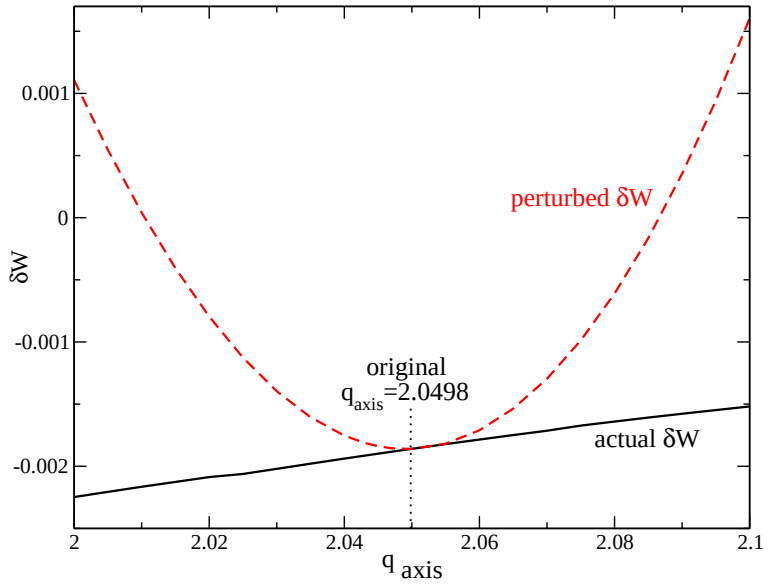

Figure 4.18: Perturbed and actual δW for perturbations about $q_{axis} = 2.0498$ of DIII-D discharge 87009. The error rapidly increases in both directions of perturbation.

as it is here, $\delta W_{perturbed}$ will no longer be minimized. It will be too large, regardless of the direction of perturbation. If the error isn't too large, the parabola would be much shallower, and results would be useful over a wider range of perturbations. The error could be corrected by using the proper $\underline{\xi}$ for each equilibrium, but that defeats the purpose of a perturbation analysis. Chapter 5 examines ways to approximate $\underline{\xi}_{perturbed}$.

4.5 Perturbations of simple idealized toroidal equilibria

Even though the perturbed stability analysis worked well for the screw pinch, results from DIII-D discharge 87009 had unacceptably large errors. Between the circular idealized equilibrium of the screw pinch and the shaped toroidal equilibrium of 87009 lie several other equilibria, which we hoped might produce intermediate results. We

planned to construct several of these intermediate equilibria, starting with a circular cross-section and making progressive changes to shape and profiles until ending at 87009. We would then try to gain some understanding about why q_{axis} in 87009 is so sensitive by perturbing q_{axis} in each of these intermediate equilibria. However, results for even the very simplest idealized toroidal plasma were disappointingly similar to those for 87009. Rather than evolving our simple toroidal equilibrium to an equilibrium similar to 87009, we focused on why the technique was producing such large errors for toroidal equilibria. Chapter 5 will explore sources of error.

To avoid any complexities that may be inherent in a real experimental equilibrium, we constructed a simple idealized toroidal equilibrium with:

- No wall, to reduce vacuum energy and wall stabilization effects,
- Circular cross-section, so shaping complexities would be eliminated,
- High aspect ratio ($r = 50$, $R = 4000$, $A = 80$), so that curvature effects would be minimized,
- $\beta = 0$, to reduce pressure terms in δW, and
- Nearly linear q profile, to minimize magnetic shear effects, and $1.05 < q < 1.9$, so there would be no integral rational surfaces. The q profile is shown in Figure 4.19.

In addition, we specified incompressibility in the stability analysis, to eliminate $\xi_{\|}$ terms in δW.

To construct this simple equilibrium and its perturbed variants, we used TOQ [16, 17]. TOQ is an equal-arc-length, inverse equilibrium solver for the Grad-Shafranov

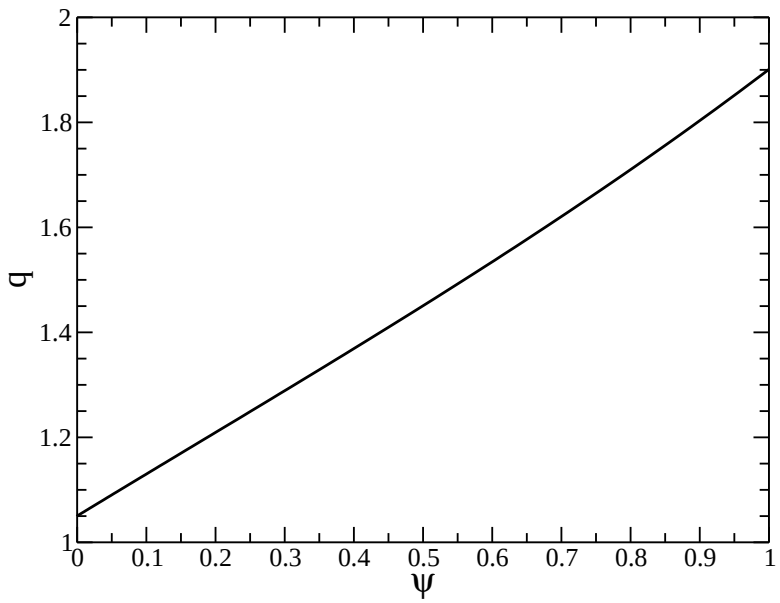

Figure 4.19: Nearly linear q profile for simple toroidal equilibrium minimizes magnetic shear effects. Also, $1.05 < q < 1.9$ eliminates $n = 1$ (integral) rational surfaces.

equation originally written and maintained at General Atomics. All equilibria produced by TOQ were also checked for proper convergence by GATO.

Being optimistic, we first varied q three different ways. Being cautious, we kept q between 1 and 2:

- For the first set of perturbations, we fixed $q_{edge} = 1.9$ but varied q_{axis} from 1.01 to 1.1.
- Next, we fixed $q_{axis} = 1.05$ and varied q_{edge} from 1.75 to 1.95.
- Finally, we shifted the entire q-profile up and down. The shape and slope did not change.

None of the three q perturbations, shown in Figure 4.20, are very large, with the possible exception of moving q_{edge} below 1.9.

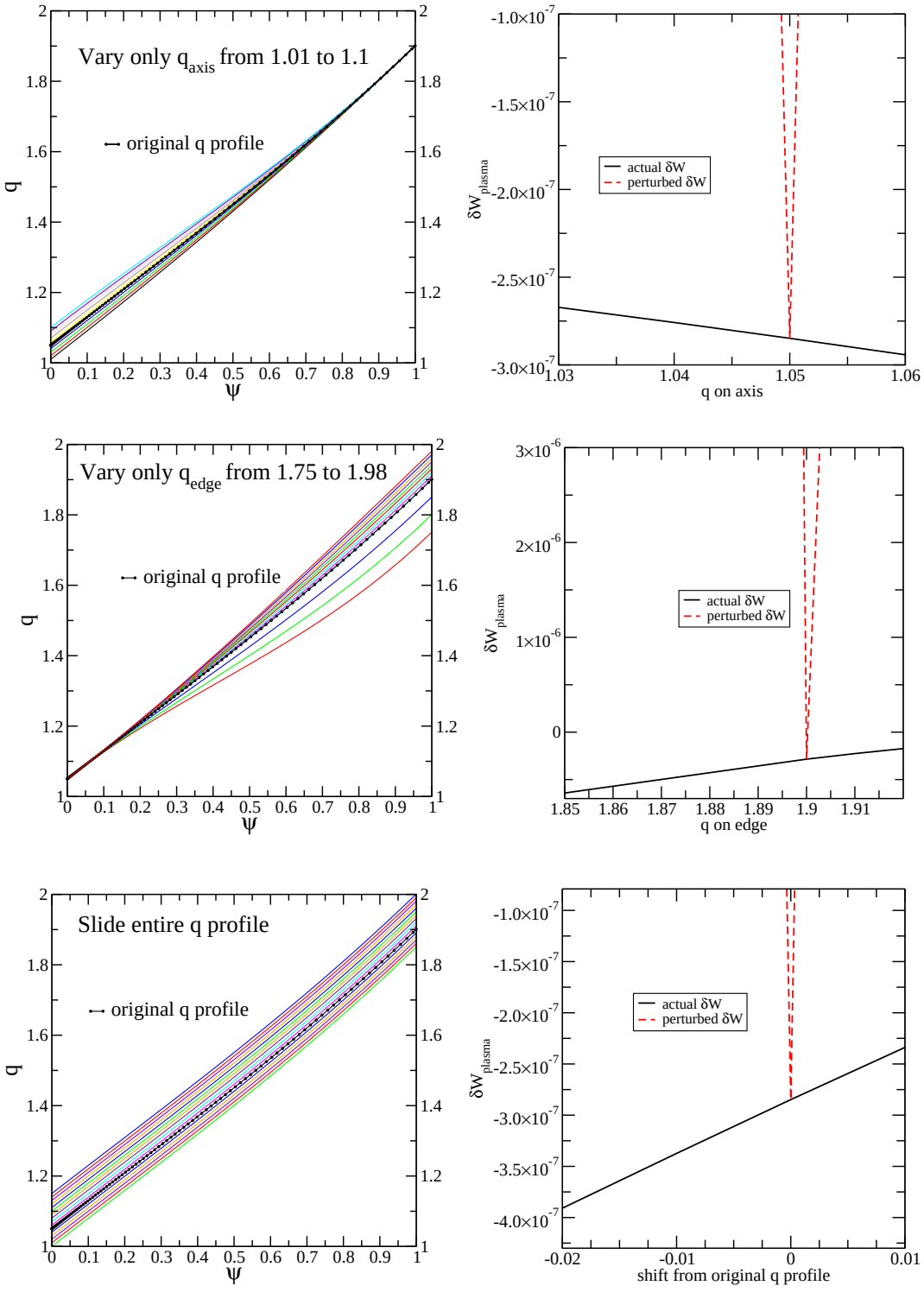

Figure 4.20: Perturbations of the q profile for the ideal toroidal equilibrium, and corresponding actual and perturbed δW.

Figure 4.20 also shows the same rapid deviation of $\delta W_{perturbed}$ from δW_{actual} as seen with the experimental equilibrium perturbations, for each of the q variations. None of the attempts stand out as considerably more successful than any other. We next looked for a simpler perturbation that would leave profiles unchanged.

The simplest equilibrium perturbation is changing the aspect ratio, varying the major radius from $R = 50$ to 5000, rather than changing the minor radius r. This does not alter the shape, the q profile, nor the magnetic fields; only curvature changes. Even though the perturbation is very simple, the perturbed stability results still quickly exhibits large errors. Figure 4.21 compares $\delta W_{perturbed}$ results for varying the aspect ratio about four different starting points: $A = 100$, $A = 60$, $A = 10$, and $A = 3$. At lower aspect ratios, δW_{actual} is more sensitive to aspect ratio. This is reflected in the steepness of the perturbed results.

For an even simpler perturbation and to check the equilibrium, we added a wall and varied the wall position, as we did for 92691 at the beginning of the chapter. Wall shape and relative position remained the same: circular and concentric with the plasma. Starting at a wall distance $D = 10r$, D was varied from almost on the plasma to infinity. Figure 4.22 shows that over this entire range, $\delta W_{perturbed}$ was very close to δW_{actual}. Agreement is even better than when moving the conformal wall with 92691's equilibrium, which confirms that our "simple" equilibrium is indeed simplified.

4.6 Computational results

The underlying goal of the perturbation technique is a substantial reduction in the time needed for comprehensive stability analyses. Even if the perturbations gave good approximations for $\Delta\delta W$, they would not be very useful if the computation time were

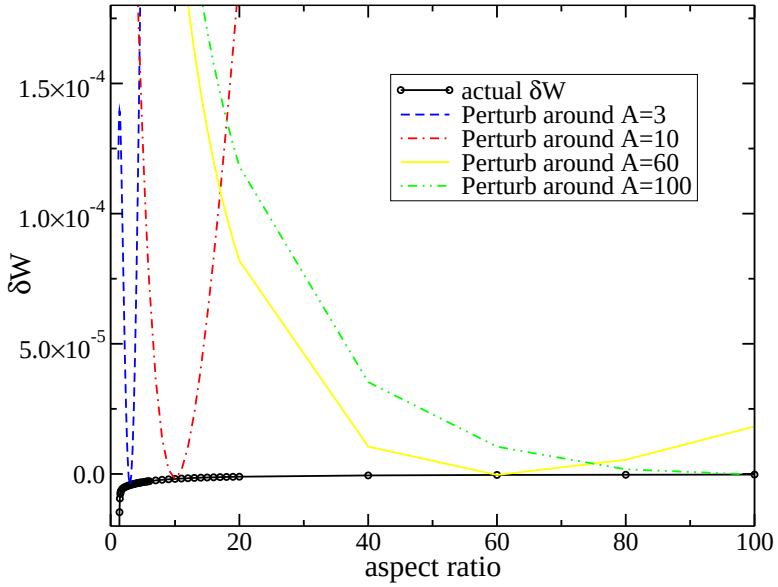

Figure 4.21: Perturbed δW results for varying the aspect ratio of a simple toroidal plasma show rapid excursion from the actual results. The error is highest where δW_{actual} is most sensitive to aspect ratio.

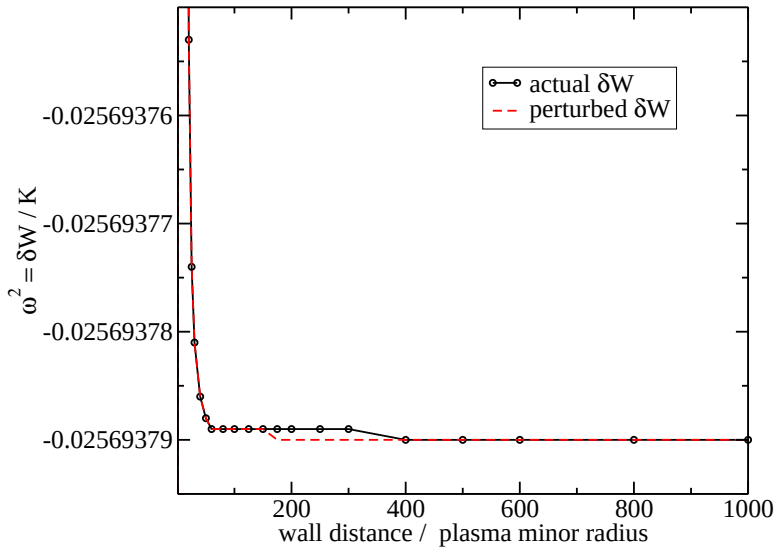

Figure 4.22: Perturbed and actual δW for variations in wall position for the simple toroidal plasma.

Stability mesh	Full ω^2		Perturbed ω^2	
65×65 Equilibrium mesh:				
60×120	$\sim$3	min	< 30	sec
100×200	5-20	min	< 1	min
129×129 Equilibrium mesh:				
60×120	4-5	min	< 30	sec
100×200	25-120	min	< 1	min
200×400	5-10	hr	< 1	min

Table 4.1: Comparison of CPU times for computing actual and perturbed δW on various platforms.

not decreased.

Table 4.1 compares average CPU times of running GATO and the perturbation code for 87009 on a 100×200 ($\psi \times \theta$) computational mesh. The times reflect typical convergence and iteration settings, and are similar on several modern platforms with various FORTRAN compilers (laptop PC running linux, J90 machines at NERSC, HP and Sun workstations running various flavors of Unix, etc). For even modest meshes, finding the eigenvector takes from 3 minutes to over 10 hours, depending on the equilibrium.

Reductions in computation time are significant: factors of 30-100 (or 97-99%) for typical calculations. These large reductions strongly motivate us to explain and decrease large errors in $\delta W_{perturbed}$.

4.7 Mixed results from perturbations of toroidal equilibria

Perturbed and actual δW agree very well when wall parameters are changed, with both experimental and simple toroidal equilibria. We successfully perturbed:

- overall wall distance for conformal walls (with $n = 0$ and $n = 1$),
- distance between the plasma and inboard, outboard, and top/bottom wall segments for a simple parameterized wall (with $n = 0$), and
- inboard wall shape for a simple parameterized wall (with $n = 0$).

In contrast, changing plasma equilibrium parameters, rather than wall parameters, consistently resulted in large errors to $\delta W_{perturbed}$. We examined perturbations to:

- the q profile for an experimental equilibrium,
- aspect ratio for a simple equilibrium, and
- q profiles for a simple equilibrium.

Perturbing only the wall parameters is a useful application of the technique, but rather limited. The possible time reductions provide a great incentive to understand the unexpected sensitivity of toroidal stability approximations to equilibrium parameter perturbations. Chapter 5 investigates the source of large errors to $\delta W_{perturbed}$, and explores methods for reducing the error.

Chapter 5

Analysis of Perturbation Errors

Chapter 4 showed very good results for $\delta W_{perturbed}$ when perturbing wall parameters. Perturbations of other parameters resulted in rapidly growing errors to $\delta W_{perturbed}$. In this chapter we explore possible sources of this error, and methods that might reduce it. We will:

- compare various forms of $\omega^2 = \dfrac{\delta W}{K}$ to verify our mathematical expansion and code,
- investigate possible sources of error from equilibrium convergence and mapping/coordinate system shifts,
- revisit the assumption of small perturbations,
- examine errors from components of δW, and finally
- explore ways to estimate $\Delta\underline{\xi}$.

None of these investigations, however, appreciably or consistently improve the error in δW. Ultimately, we are faced with a classic problem in numeric physics: looking for a very small difference between extremely large numbers.

5.1 Comparison of forms of $\omega^2 = \dfrac{\delta W}{K}$

In Chapter 2, we dropped all second order terms of the perturbed expansion of $\omega^2 = \dfrac{\delta W}{K}$, and also neglected changes to the kinetic energy K to arrive at Equation (2.11):

$$\Delta\delta W = -\tfrac{1}{2}\int \underline{\xi}^* \cdot \Delta\underline{F}(\underline{\xi})\; d^3r.$$

Comparing various forms of the expansion for ω^2 to the computed actual ω^2 gives a rough indication of the origin of the error. For each of the following comparisons, we use the simple toroidal equilibrium and perturb the aspect ratio about $A = 80$. Stability is very insensitive to aspect ratio at this very high value, so we may safely associate any findings with the technique rather than with changes in stability.

We first compare ω^2_{actual} computed by GATO and $\dfrac{\delta W_{actual}}{K_{actual}}$, with δW_{actual} and K_{actual} produced by matrix multiplication. The two agree exactly, confirming that the matrix calculation correctly treats the vacuum energy.

We next compare ω^2_{actual} computed by GATO and the complete expansion of $\dfrac{\delta W}{K}$ (Equation (2.7)), using newly computed $\underline{\xi}$ where needed:

$$\begin{aligned}\omega^2 + \Delta\omega^2 = -\tfrac{1}{2}\int d^3r\, \big[&\underline{\xi}^*\cdot\underline{F}(\underline{\xi}) + \Delta\underline{\xi}^*\cdot\underline{F}(\Delta\underline{\xi}) + 2\Delta\underline{\xi}^*\cdot\underline{F}(\underline{\xi}) + \underline{\xi}^*\cdot\Delta\underline{F}(\underline{\xi}) + \\ &2\Delta\underline{\xi}^*\cdot\Delta\underline{F}(\underline{\xi}) + \Delta\underline{\xi}^*\cdot\Delta\underline{F}(\Delta\underline{\xi})\big] \quad / \\ &\big[\rho|\underline{\xi}|^2 + \Delta\rho|\underline{\xi}|^2 + 2\rho|\underline{\xi}\cdot\Delta\underline{\xi}| + 2\Delta\rho|\underline{\xi}\cdot\Delta\underline{\xi}| + \rho|\Delta\underline{\xi}|^2 + \Delta\rho|\Delta\underline{\xi}|^2\big]\,.\end{aligned}$$

These forms of ω^2 agree exactly as well, so we may conclude that the expansion is mathematically correct and the terms are being computed properly.

Next we check the assumption that ΔK can be neglected. We compare $\dfrac{\delta W_{actual}}{K}$ using three different values for K:

- Actual $K = \int \rho_{actual}|\underline{\xi}_{actual}|^2\; d^3r$. This gives ω^2_{actual}.

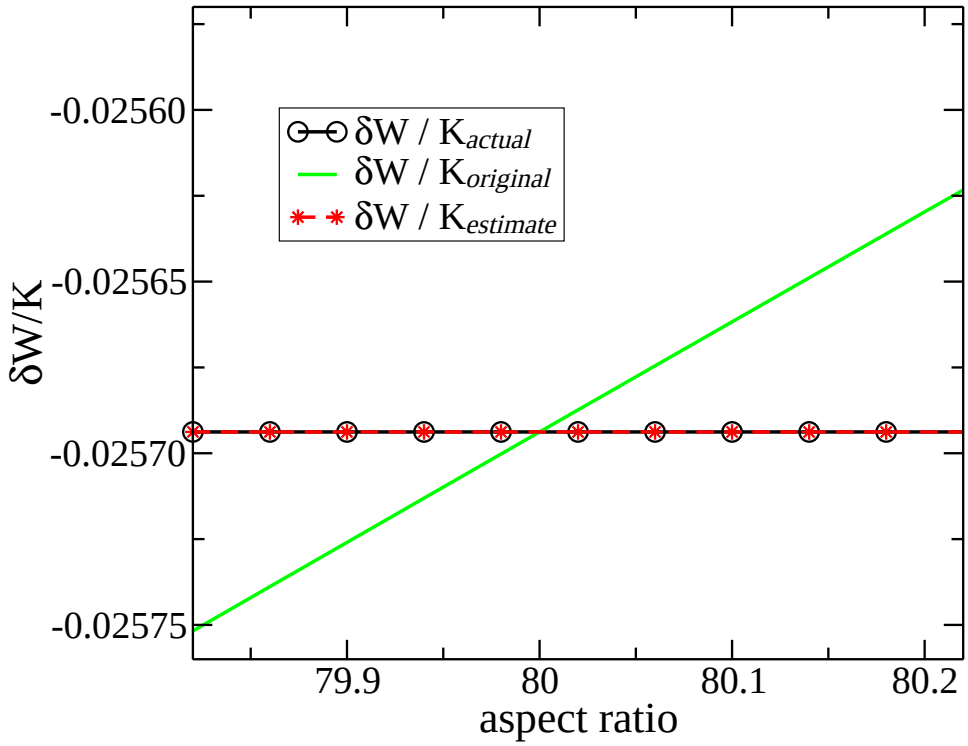

Figure 5.1: Comparison of $\frac{\delta W_{actual}}{K}$ using K_{actual}, $K_{original}$, and $K_{estimate}$ shows that neglecting changes in K is not valid, but approximating K is adequate.

- Original $K = \int \rho_{original} |\underline{\xi}_{original}|^2 \, d^3r$. This is equivalent to neglecting changes in K.

- Estimated $K = \int \rho_{actual} |\underline{\xi}_{original}|^2 \, d^3r$. This approximation is analogous to approximating $\delta W = -\frac{1}{2} \int \underline{\xi}^* \cdot \Delta \underline{F}(\underline{\xi}) \, d^3r$.

In Figure 5.1, results with K_{actual} and $K_{estimated}$ agree quite well, while $K_{original}$ "tilts" ω^2 counterclockwise. Neglecting ΔK, therefore, is not correct. Estimating K, however, is adequate. The approximation must be included, but it is easily computed. Even though ρ does not change in these perturbations, the change in aspect ratio affects the Jacobian. This coordinate change produces ΔK.

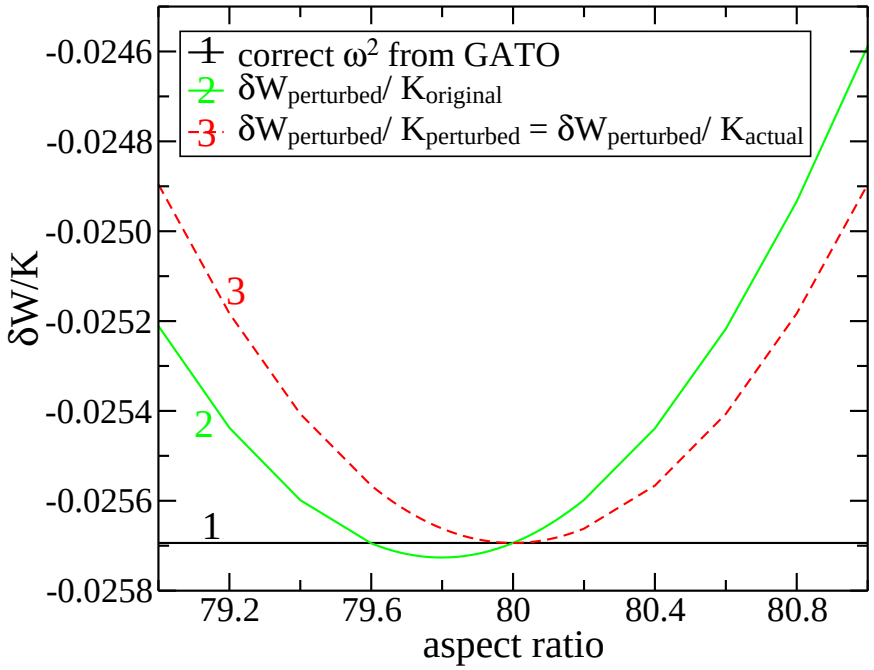

Figure 5.2: Comparison of ω^2, $\frac{\delta W_{estimate}}{K_{original}}$, and $\frac{\delta W_{estimate}}{K_{estimate}}$ shows that using $K_{estimate}$ somewhat improves results, but does not overcome errors in $\delta W_{estimate}$.

Finally, we determine if neglecting ΔK is solely responsible for the large errors with the simple and experimental equilibria. Unfortunately, Figure 5.2 shows that properly estimating K still results in a poor estimate for ω^2 (now using $\delta W_{estimate}$). While using the correct K is important, it is not enough to compensate for δW being correctly approximated over only a very small range of $A = 79.96$ to $A = 80.04$.

5.2 Examination of second order terms in δW expansion

With the expansion confirmed and the relative importance of ΔK determined, we now examine all of the terms in the complete expansion of $\delta W + \Delta\delta W$:

$$\delta W + \Delta\delta W = -\tfrac{1}{2}\int d^3r$$
$$[\,\underline{\xi}\cdot\underline{F}(\underline{\xi}) + 2\Delta\underline{\xi}\cdot\underline{F}(\underline{\xi}) + \Delta\underline{\xi}\cdot\underline{F}(\Delta\underline{\xi}) +$$
$$\underline{\xi}\cdot\Delta\underline{F}(\underline{\xi}) + 2\Delta\underline{\xi}\cdot\Delta\underline{F}(\underline{\xi}) + \Delta\underline{\xi}\cdot\Delta\underline{F}(\Delta\underline{\xi})\,]$$

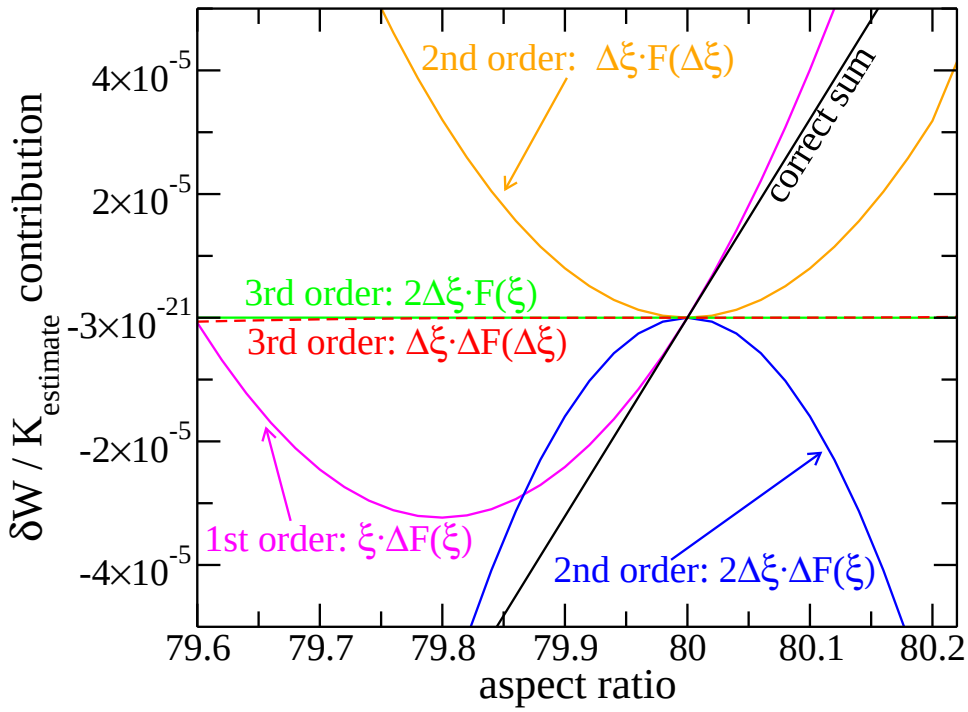

Figure 5.3: First, second and third order terms of $\delta W + \Delta\delta W$ expansion perturbed about $A = 80$. Second order terms are not negligible.

No terms containing $\Delta\underline{\xi}$ are included in the perturbation, but it is possible that the second or third order terms are in fact *not* negligible. Figure 5.3 compares the terms

(normalized with $K = \int \rho_{actual} |\underline{\xi}_{original}|^2 d^3r$) as aspect ratio is very slightly perturbed about $A = 80$. The plot shows:

- The third order term $\Delta\underline{\xi} \cdot \Delta\underline{F}(\Delta\underline{\xi})$ and first order term $\Delta\underline{\xi} \cdot \underline{F}(\underline{\xi})$ are small. The third order term can be safely neglected.

- The first order term $\underline{\xi} \cdot \Delta\underline{F}(\underline{\xi})$ changes linearly near $A = 80$, but quickly becomes non-linear and grows faster with larger perturbations. This is the single term used in the $\delta W_{perturbed}$ calculations.

- The second order terms containing $\Delta\xi$ do become quite large. The second order terms $2\Delta\underline{\xi} \cdot \Delta\underline{F}(\underline{\xi})$ and $\Delta\underline{\xi} \cdot \underline{F}(\Delta\underline{\xi})$ grow quadratically near the perturbation center, becoming extremely large with even very small perturbations. Their signs are opposite, but they do not quite cancel. This small difference between two large numbers is needed to correct the first order approximation. As the perturbation grows, the "small" difference becomes significant.

5.3 Possible sources of error from equilibria and coordinate system

We next examined possible sources of error from the equilibria. Our simple toroidal equilibria were produced by TOQ. In some situations, TOQ may not converge on a solution, but will still produce an equilibrium. Using a faulty equilibrium would certainly produce errors. As a safeguard, GATO verifies the convergence of its input equilibrium. Equilibria convergence recomputed by GATO were all well within acceptable limits.

A change in the location of the magnetic axis of the equilibrium might also produce errors. As aspect ratio varies, the Shafranov shift is also expected to move. A large

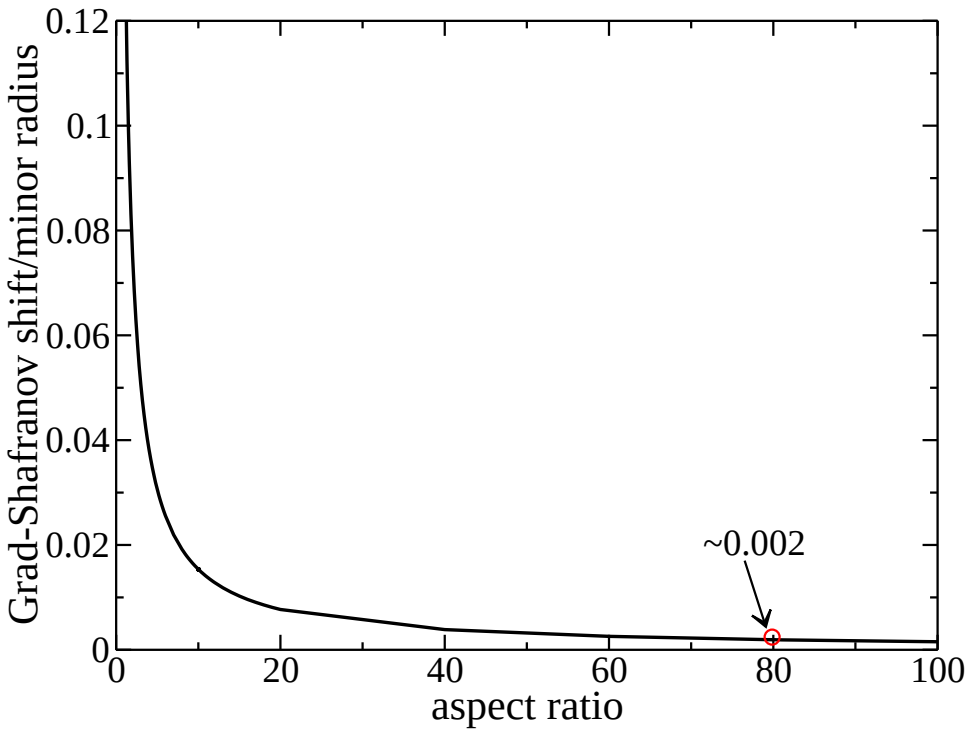

Figure 5.4: Shafranov shift of simple toroidal equilibrium (normalized to minor radius) is small and changes little for most aspect ratios.

difference in the shift could alter the $\underline{\xi}$ mapping. However, Figure 5.4 shows that the magnetic axis shift is very small, and changes very little above $A \approx 20$. At $A = 80$, where we centered the perturbations, the shift (normalized to minor radius) is only 0.002.

In addition, all equilibria used the same (ψ, θ) mesh packing and same initial mapping for $(\psi, \theta) \mapsto (r, z)$. Also, $\underline{\xi}$ is on the (ψ, θ) mesh of the original equilibrium, and remains on that mesh. These mesh consistencies further ensure that $\underline{\xi}$ for a given flux surface will still map to that flux surface, even if the surface moves in (r, z) space.

We have also tested perturbations (aspect ratio, q_{axis}) that, when consistent mapping and flux surface packing are also used, do not change the basis functions. (Basis

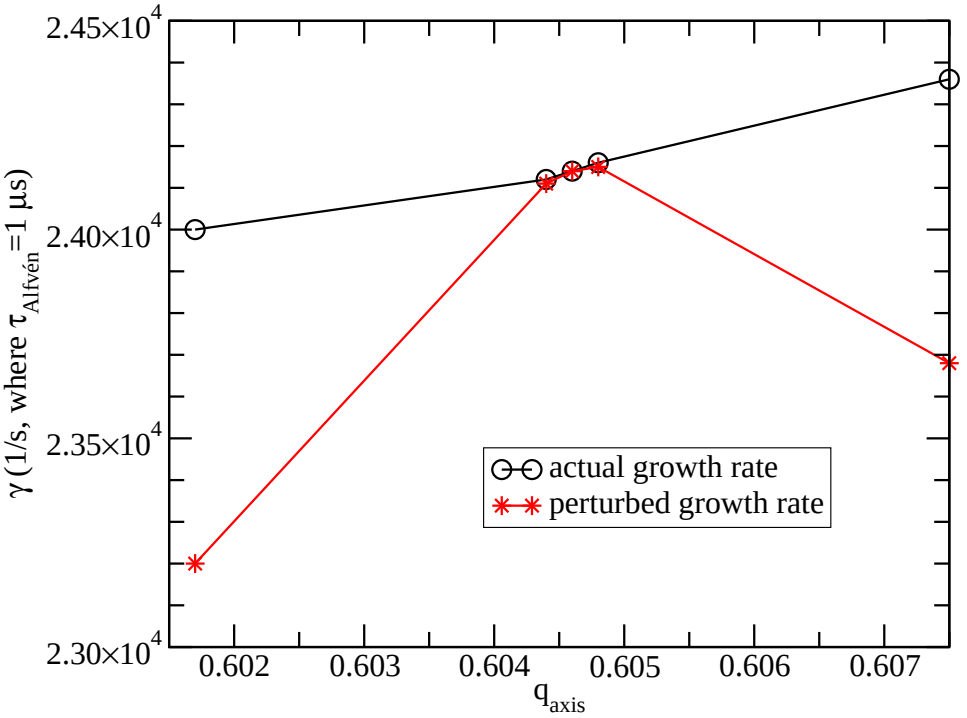

Figure 5.5: Actual and perturbed growth rates obtained with NIMROD for perturbing q_{axis} have same trend as those obtained with GATO.

function sensitivity was discussed in Chapter 2.) To confirm that our coordinate system was not changing, Carl Sovinec repeated some perturbations with the code NIMROD [40], a sophisticated non-linear MHD solver. Equilibrium quantities may be directly perturbed in NIMROD without affecting the coordinate system, and linear (as well as non-linear) MHD growth rates may be obtained.

Results from repeating our q_{axis} perturbations are shown in Figure 5.5. While growth rate rather than δW is shown, the same trend (increasing error with increasing perturbation) is evident. The care taken to not change the basis functions in the NIMROD calculations confirms that coordinate system shifts (re-using $X_{original}$ rather than strictly $\underline{\xi}_{original}$) are not responsible for the perturbations' sensitivity. Similar NIMROD calculations also reveal that when the compressional Alfvén energy is included

in the screw pinch analysis, rapidly increasing errors are also seen.

5.4 Assumption of small perturbations

We next verified that our perturbations were in fact small. If $\Delta|\underline{\xi}|/|\underline{\xi}|$ and $\Delta|\underline{F}|/|\underline{F}|$ are not both small and of same order of magnitude, then the premise of a small perturbation is flawed, and we cannot justify neglecting the second and third order terms in the expansion of δW.

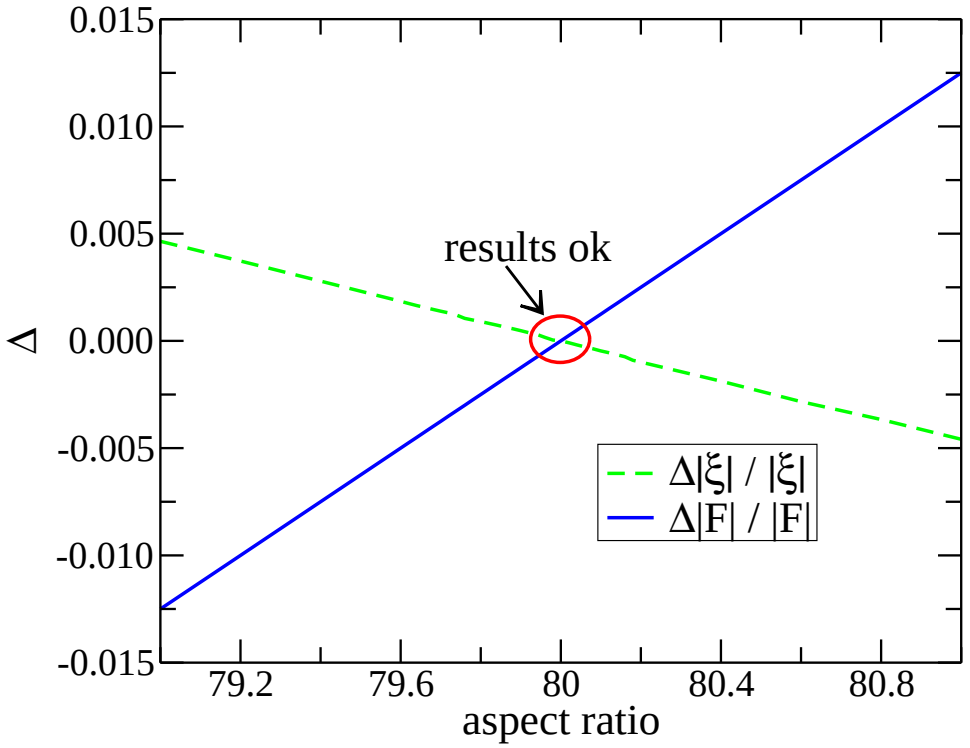

Figure 5.6: Normalized perturbations are both very small near $A = 80$.

Figures 5.6 and 5.7 compare $\Delta|\underline{\xi}|/|\underline{\xi}|$ and $\Delta|\underline{F}|/|\underline{F}|$ both near the center of perturbations at $A = 80$, and much farther away. Near $A = 80$, both $\Delta|\underline{\xi}|/|\underline{\xi}|$ and $\Delta|\underline{F}|/|\underline{F}|$

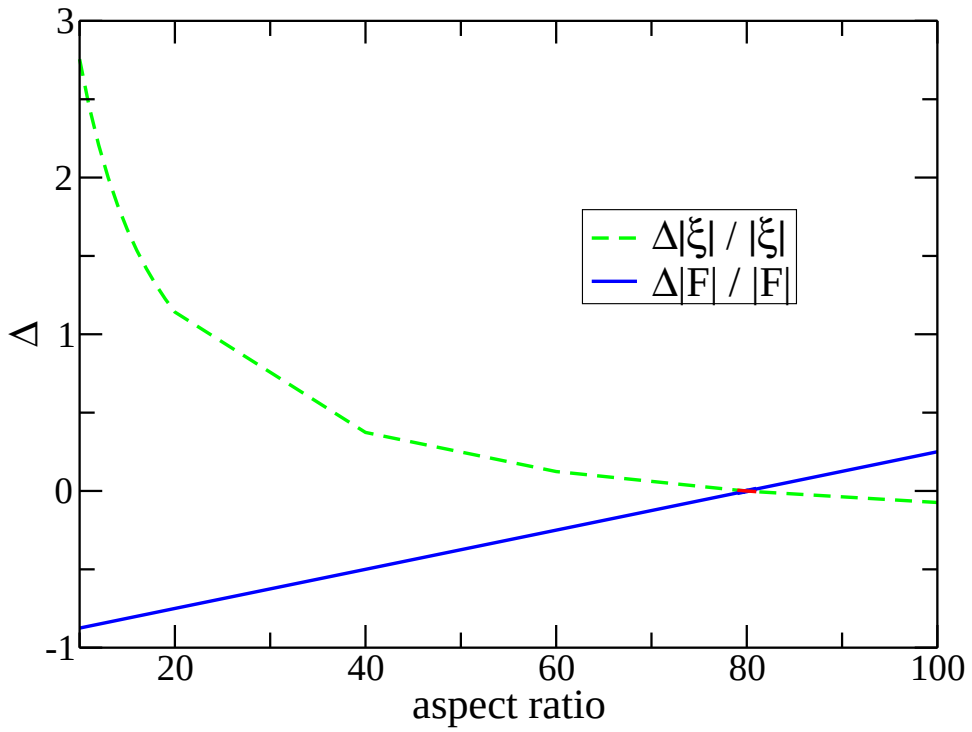

Figure 5.7: Normalized perturbations become large far from $A = 80$, but F remains linear.

are very small: $\approx 10^{-3}$ to 10^{-2}. Still, the perturbation technique only produces acceptable results when $\Delta|\underline{\xi}|/|\underline{\xi}|$ and $\Delta|\underline{F}|/|\underline{F}| <$ 1-2 $\times 10^{-3}$. Both $\Delta|\underline{\xi}|/|\underline{\xi}|$ and $\Delta|\underline{F}|/|\underline{F}|$ are linear with aspect ratio over a wide range. Far away from $A = 80$, both $\Delta|\underline{\xi}|/|\underline{\xi}|$ and $\Delta|\underline{F}|/|\underline{F}|$ become quite large, although $|\underline{F}|$ remains linear. This enticingly suggests finding a simple relationship between $\Delta\underline{\xi}$ and $\Delta\underline{F}$ might be possible. However, we were unable to discover such a relationship.

5.5 Errors from large δW component

We also examined each component of $\delta W_{perturbed}$ computed by GATO. The energy components are represented in GATO coordinates, and they are not quite the same

as their counterparts given by Furth, Killeen, Rosenbluth and Coppi [20] (Equation (2.16)):

- δW_1: destabilizing energy (roughly corresponds to most of the pressure-driven interchange and current-driven kink terms of Equation (2.16)).
- δW_2: normal magnetic field line bending energy (roughly corresponds to most of the shear Alfvén term).
- δW_3: cross (∼poloidal) magnetic field line bending energy (contains parts of the shear Alfvén term and the current-driven kink term).
- δW_4: parallel magnetic field line bending energy (roughly corresponds to fast compressional Alfvén term, plus part of the pressure-driven interchange term).
- δW_5: acoustic compression energy (corresponds exactly to acoustic term).

All terms except δW_4, which is almost the fast compressional Alfvén term (or δW_{FCA}), changed very little as $A = 80$ was perturbed, as shown in Figure 5.8. The fast compressional Alfvén energy usually becomes small, but only through cancellations. In computing δW_{FCA}, some coefficients of $\underline{\xi}$ can be much larger than those appearing in other δW components:

$$\frac{r^2}{\mathcal{J}}, \qquad \frac{f\mathcal{J}}{r^2}, \qquad \frac{1}{\mathcal{J}}, \qquad f\frac{\partial}{\partial\psi}\frac{\mathcal{J}}{r^2},$$

where r is the minor radius and $\mathcal{J}$ is the Jacobian. Because of these large coefficients, cancellation can catastrophically fail if $\underline{\xi}$ is incorrect. Converting from GATO coordinates to field line coordinates used in Equation (2.16) yields the same trends in δW components: the error is from the fast compressional Alfvén term.

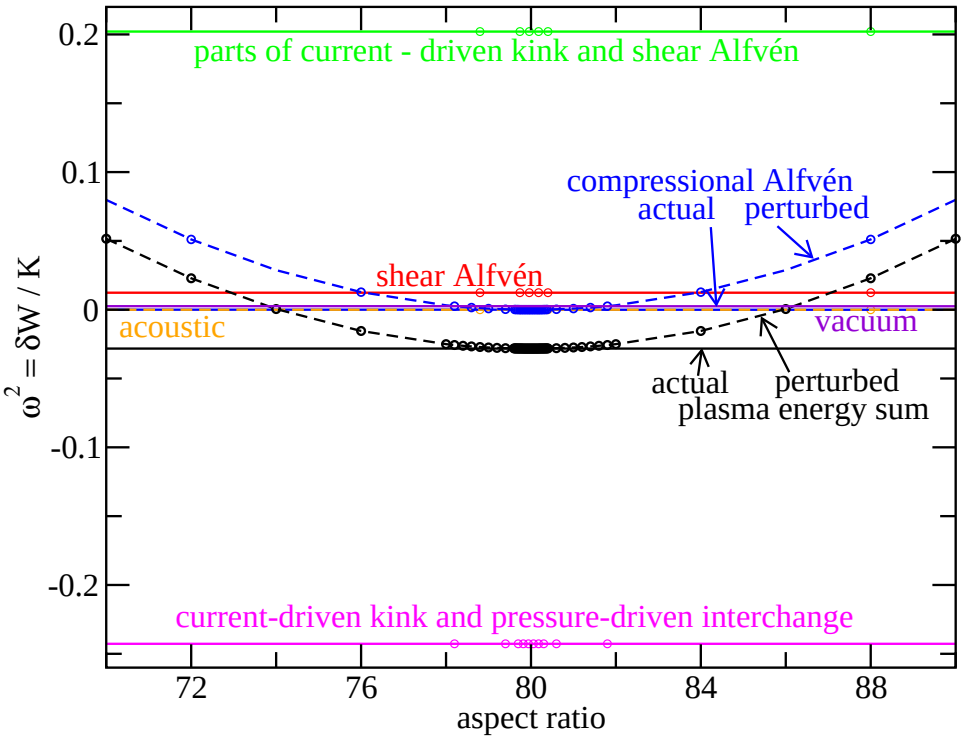

Figure 5.8: All δW components change very little as aspect ratio is perturbed, except fast compressional Alfvén term.

The eigenvalue problem $A\underline{x} = \omega^2 B\underline{x}$ contains very stiff, sparse matrices A and B. Terms in A range from 10^{-5} to 10^{9}, with most of the extreme variation originating in δW_{FCA}. The proper calculation of δW relies on near-cancellation of very large numbers (of order 10^4 to 10^9) to balance and further cancel with much smaller numbers (of order 10^{-5} to 10^{-1}). If the large numbers are perturbed only even a hundredth of a percent, this change will still ruin cancellation with the smaller numbers.

The successful screw pinch results also support the claim that the increasing error is due to sensitivity in the fast compressional Alfvén term. The screw pinch analysis used a form of the Lagrangian that analytically eliminated compressional Alfvén energy. Screw pinch calculations with NIMROD (including the compressional Alfvén energy)

showed the same increasing error as is seen in the toroidal GATO results.

5.6 Estimating $\Delta\xi$

Better cancellation of the fast compressional Alfvén energy term requires a more correct $\underline{\xi}$. But $\underline{\xi}$ comes from GATO, and the point of running the perturbations is to *not* rerun GATO. We might try to change $\underline{F}$ to improve cancellation, but this would alter the equilibrium. Our perturbed stability results would no longer apply to our equilibrium. Instead, we try to estimate $\Delta\underline{\xi}$ by minimizing δW_{FCA} rather than all of δW. For the simplest minimization, we determine what $\underline{\xi}$ would be at each mesh point if the fast compressional Alfvén energy (δW_{FCA}) remained close to its local unperturbed value:

$$\delta W_{FCA,perturbed}(\underline{\xi}_{estimate}) = \delta W_{FCA,original}(\underline{\xi}_{original}) \tag{5.1}$$

within some small but non-zero tolerance. Numerical representation of δW_{FCA} is linear and periodic, making this estimate straightforward:

$$\delta W_{FCA} = aX + b\frac{\partial X}{\partial \psi} + c\frac{\partial U}{\partial \theta}, \tag{5.2}$$

where a, b and c are coefficients determined by the equilibrium, and x and u are finite element representations of $\xi_{\|}$ and ξ_{θ}. We now have an estimate of $\Delta\underline{\xi}$:

$$\Delta\underline{\xi} = \underline{\xi}_{original} - \underline{\xi}_{estimate}. \tag{5.3}$$

For our simple toroidal equilibrium with high $A = 80$, using the estimated $\underline{\xi}$ while perturbing A gives much better results for δW. Figure 5.9 compares δW_{actual}, $\delta W_{perturbed}$ using $\underline{\xi}_{original}$, and $\delta W_{perturbed}$ using $\underline{\xi}_{estimate}$, showing a significant improvement with $\underline{\xi}_{estimate}$.

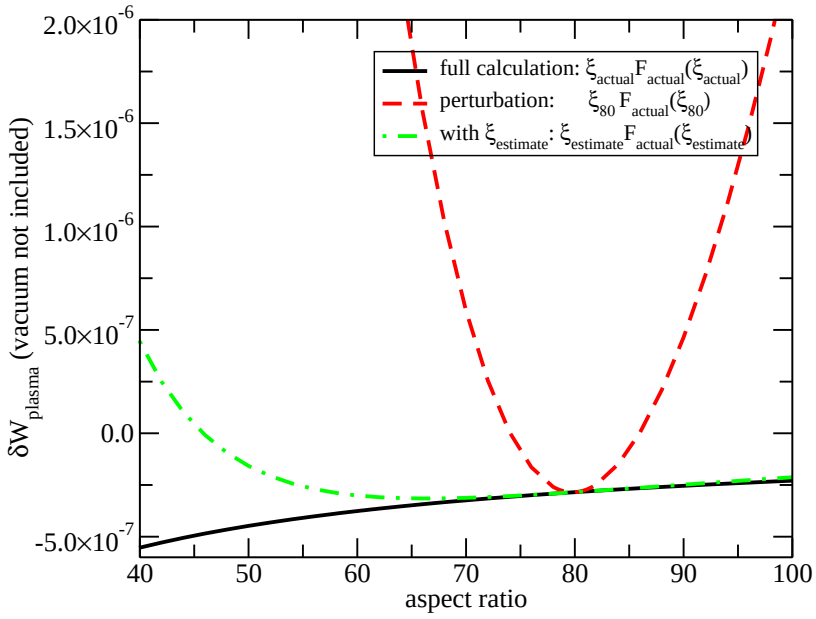

Figure 5.9: Using $\xi_{estimate}$ in $\delta W_{perturbed}$ while perturbing aspect ratio about $A = 80$ improves results.

Perturbations are next made about a lower $A = 10$, where stability is more sensitive to aspect ratio. Using $\underline{\xi}_{estimate}$ now gives only a slight improvement to $\delta W_{perturbed}$, as shown in Figure 5.10.

Using $\underline{\xi}_{estimate}$ with the perturbed q profiles of the simple toroidal equilibrium also offers only a slight improvement to $\delta W_{perturbed}$. Although results with $\underline{\xi}_{estimate}$ graphically appear much better, the range of allowable perturbations is still quite small. Figures 5.11, 5.12, and 5.13 show this apparent improvement when perturbing q_{axis} and q_{edge}, and when shifting the entire q profile.

If the energy components are examined for each of these perturbations, δW_{FCA} changes very little, as expected. But the error is now shifted to other components of δW. The error is reduced somewhat, but is still present.

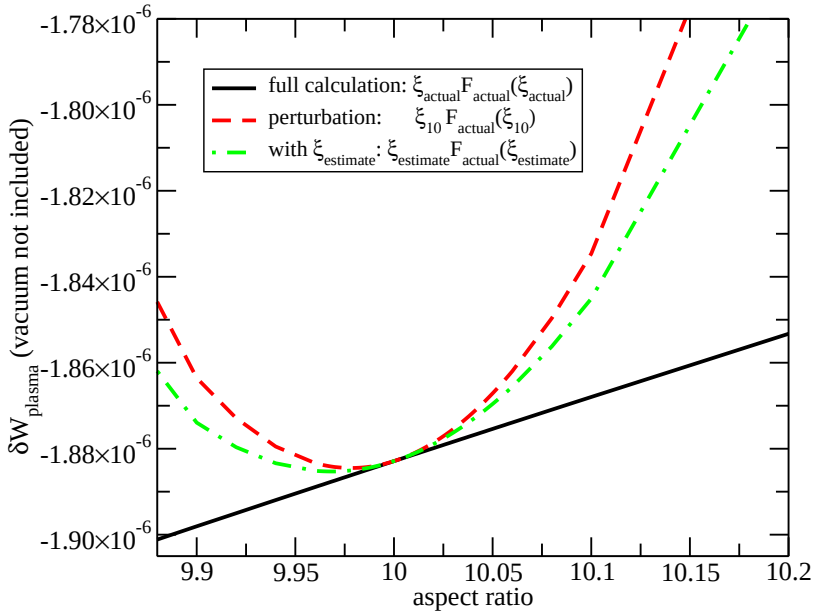

Figure 5.10: Using $\xi_{estimate}$ in $\delta W_{perturbed}$ while perturbing aspect ratio about $A = 10$ only slightly improves results.

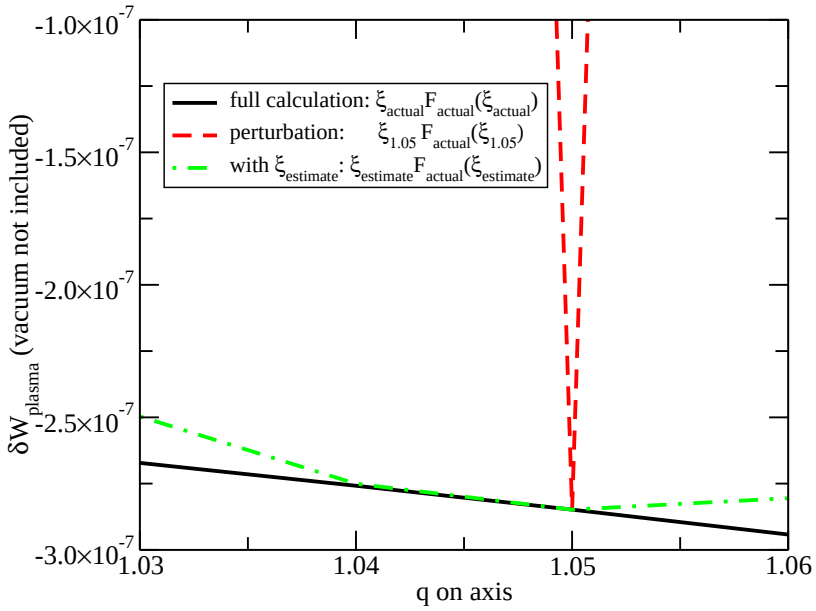

Figure 5.11: Using $\xi_{estimate}$ in $\delta W_{perturbed}$ while perturbing q_{axis} appears to significantly improve $\delta W_{perturbed}$, but the range of allowable perturbations is still very small.

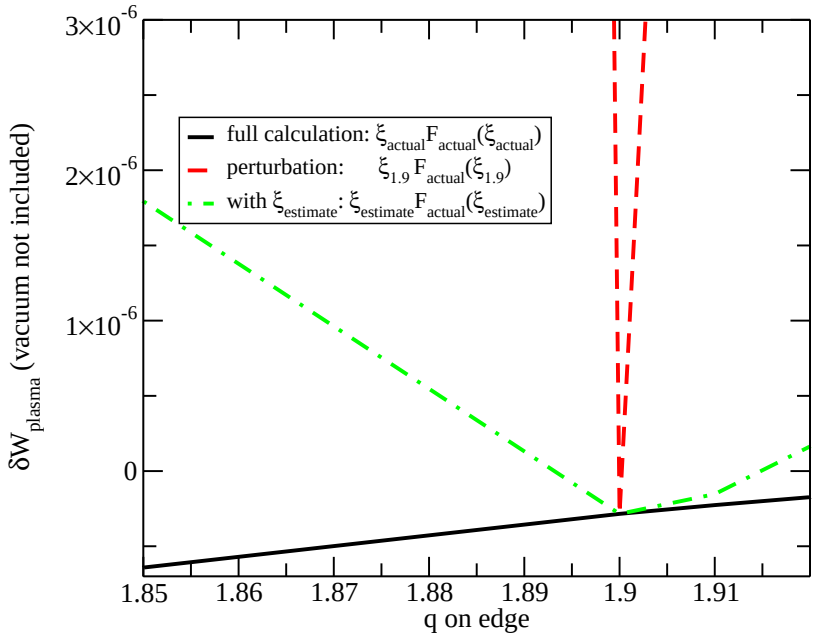

Figure 5.12: Using $\xi_{estimate}$ in $\delta W_{perturbed}$ while perturbing q_{edge} slightly improves $\delta W_{perturbed}$.

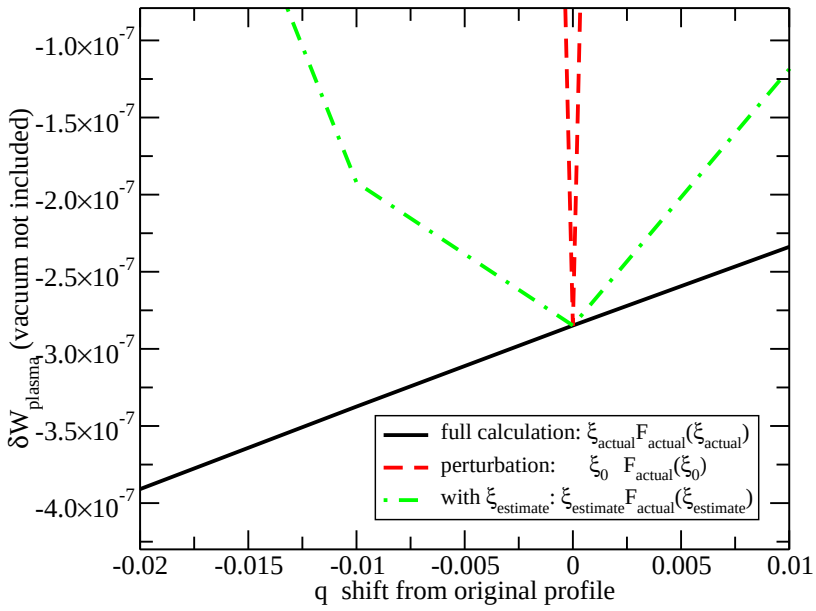

Figure 5.13: Using $\xi_{estimate}$ in $\delta W_{perturbed}$ while shifting q profile offers some improvement to $\delta W_{perturbed}$, but the range of allowable perturbations is still small.

The error might be further reduced with a more rigorous minimization of δW_{FCA}, which might give a better estimate of $\Delta\underline{\xi}$. Rather than simply requiring δW_{FCA} to remain close to its unperturbed value, we would solve two additional eigenvalue problems. For the first new eigenvalue problem, we would find the displacements $\underline{\xi}_{FCA}$ that would result if δW_{FCA} were the only plasma energy contribution to the potential energy matrix A (with the original equilibrium) in the eigenvalue problem of Equation (4.1):

$$A_{FCA}\xi_{FCA} = \omega^2_{FCA}B\xi_{FCA}. \tag{5.4}$$

Next, we would perturb the original equilibrium, which immediately gives perturbed matrices $\tilde{A}$ and $\tilde{B}$. Using these new perturbed matrices, we would then solve the second new eigenvalue problem for the perturbed displacements $\tilde{\xi}_{FCA}$:

$$\tilde{A}_{FCA}\tilde{\xi}_{FCA} = \tilde{\omega}^2_{FCA}\tilde{B}\xi_{FCA}. \tag{5.5}$$

We would now have $\Delta\xi_{FCA} = \xi_{FCA} - \tilde{\xi}_{FCA}$, which we could use as an estimate for $\Delta\xi_{perturbed}$:

$$\Delta\xi_{perturbed} \approx \xi_{FCA} - \tilde{\xi}_{FCA}. \tag{5.6}$$

Solving the two additional eigenvalue problems is only worthwhile if it can be done significantly faster than solving directly for $\xi_{perturbed}$. The matrix A would need to have a simpler structure that could be exploited. Keeping only δW_{FCA} plasma energy contributions to A removes all equations containing both real and imaginary components of $\underline{\xi}$ (for example, there are no $\Re(\xi_\psi)\Im(\xi_\chi)$ cells in the matrix). However, all equations containing purely real or purely imaginary components are retained (so there are still $\Re(\xi_\psi)\Re(\xi_\chi)$ cells). Assuming incompressibility, this reduces the non-zero cells of A by almost half – but does not change A's overall structure or complexity.[1]

[1]The structure of A is complicated, and is described in Appendix A.

Because A can not be appreciably simplified, obtaining an estimate for $\Delta\xi_{perturbed}$ by solving the two additional eigenvalue problems takes longer than running GATO with the perturbed equilibrium and obtaining $\xi_{perturbed}$ directly. If δW_{FCA} were the *only* contribution to A, then the matrix would be much easier to solve. However, the vacuum energy contributions must also be retained, so that boundary conditions remain consistent. The vacuum energy contribution is represented as a Green's function, with every point on the wall interacting with every point on the plasma surface. These (θ_{wall}, $\theta_{surface}$) interactions complicate A's structure, but cannot be discarded.

The structure of A also precludes solving an expansion of the eigenvalue problem for $\Delta\xi$ (similar to the technique used by Hudson *et al.*[29]):

$$(\omega^2 + \Delta\omega^2)(A + \Delta A)(\xi + \Delta\xi) = (B + \Delta B). \tag{5.7}$$

An estimate for $\omega^2 + \Delta\omega^2$ could be easily obtained from the first approximation of $\delta W_{perturbed}$ and $K_{perturbed}$:

$$(\omega^2 + \Delta\omega^2) = \frac{\delta W_{perturbed}}{K_{perturbed}}. \tag{5.8}$$

Solving Equation (5.7), however requires inverting A, which, again, is not a computational shortcut. This approach works for Hudson *et al.* because their eigenproblem involves only a single field line and easily invertable matrices.

5.7 Stability properties of numeric toroidal equilibria remain very sensitive to parameter perturbation

Our technique produces very good estimates of $\delta W_{perturbed}$ when perturbing screw pinch equilibrium parameters (with compressional Alfvén energy eliminated) or toroidal wall parameters. In contrast, errors in $\delta W_{perturbed}$ quickly increase when toroidal plasma equilibrium parameters are perturbed. We explored several possible sources this error:

- Comparisons of various forms of $\omega^2 = \frac{\delta W}{K}$ verified that our mathematical expansion, matrix multiplication, and treatment of the vacumm energy are correct. These comparisons also indicated that ΔK slightly improves results, but do not appreciably reduce the growth of the error.

- Inspection of the terms in the δW expansion indicate that second order terms are in fact quite large.

- Comparison with NIMROD calculations and examination of equilibrium convergence, magnetic axis shifts, and mapping procedures give us confidence that our equilibrium and coordinate system conversions do not contain inherent inconsistencies that might allow the second order terms to grow.

- For the equilibria we perturbed, our assumption of small perturbations is valid. Large perturbations might account for the observed large second order terms, but that is not the case here.

- Investigation of the plasma energy components of δW associate the large second

order terms with the fast compressional Alfvén energy. These terms have relatively large coefficients, but normally cancel when $\underline{\xi}$ is correct. Errors were not evident in the screw pinch analysis because the compressional Alfvén energy was analytically eliminated from δW.

- Attempts to estimate $\Delta\underline{\xi}$ with a simple minimization of the fast compressional Alfvén energy do not consistently reduce the error to an acceptable level. The error may be significantly reduced when a reasonably insensitive parameter (such as high aspect ratio) is perturbed. In general, however, correcting the fast compressional Alfvén energy transfers the error to other energy components.

- More rigorous minimizations of the fast compressional Alfvén energy might decrease the error, but would take more time than simply re-running the stability code and skipping the perturbation technique.

None of these efforts ultimately produced better estimates of δW. Changes in $\underline{\xi}$ might be considered as well, but are very difficult to estimate numerically.

Chapter 6

Summary

We have introduced a new perturbative technique with the goal of rapidly exploring the dependence of long wavelength ideal MHD instabilities on equilibrium profiles, shaping properties, and wall parameters. Traditionally, these relations are studied with numerical parameter scans using computationally intensive stability codes. The perturbative technique first finds the equilibrium and stability of an axisymmetric configuration using traditional methods. Subsequent small changes in the original equilibrium profiles, shaping properties, and wall parameters result in new stability properties for the perturbed conditions, which we find with an expansion of the energy principle. With this approach, the effects of parameter variations on stability can in theory be efficiently examined without numerically generating complete MHD stability results for every set of parameters (which can be time intensive for accurate representations of many configurations).

The theory and computational steps involved in finding stability conditions of perturbed equilibria were detailed in Chapter 2, and are outlined briefly here:

1. Obtain stability properties (potential energy δW and displacements $\underline{\xi}$) for an initial set of parameters.

2. Perturb the initial set of parameters.

3. Combine the initial stability properties and perturbed equilibrium in the perturbed energy principle.

4. Solve the perturbed energy principle for the perturbed stability $\delta W_{perturbed}$.

The equations for a screw pinch can be solved analytically, and we examined this geometry in Chapter 3. Perturbing screw pinch equilibria consistently led to accurate predictions of δW, and no major obstacles were uncovered. Because the compressional Alfvén energy was analytically eliminated from δW, the results were not a complete test of the technique. The exploration found that:

- For flat pressure and current profiles, the stability is correctly predicted over the entire wide range of pressure perturbations ($p/p_0 = 0.1$ to 2.0).

- For curved pressure and flat current profiles, the stability is correctly predicted when the pressure profile is made steeper or shallower ($p/p_0 = 1-(r/R_0)^{\alpha_3}, \alpha_3 =$ 3/2 to 5/2).

- For stepped current profiles with either curved or flat pressure profiles, the stability trends are correct over a wide range of step heights.

- For curved pressure and current profiles that exhibit high edge magnetic shear and contain $q = 1$ surfaces, displacements are not as inconsistent between the original and perturbed equilibria as initially suspected. Only small regions of the plasma are affected.

Predicting stability properties of perturbed toroidal equilibria requires numeric techniques. Both experimental and idealized equilibria were perturbed. Stability properties were successfully predicted from perturbed toroidal equilibria when only the vacuum beyond the plasma was perturbed (through wall parameter perturbations), rather

than the plasma itself. We successfully perturbed:

- overall wall distance for conformal walls (with $n = 0$ and $n = 1$),
- distance between the plasma and inboard, outboard, and top/bottom wall segments for a simple parameterized wall (with $n = 0$), and
- inboard wall shape for a simple parameterized wall (with $n = 0$).

The wall perturbations revealed two particularly useful applications:

- Positive δW pose no problem to the technique, although they can significantly increase computation time with a full stability code. Marginal stability, therefore, is much easier to find with the perturbative technique.
- Convergence of a full stability code depends on the initial guess given for the eigenvalue, which the user must supply as an input parameter. If an investigator wants to know δW_{actual}, rather than $\delta W_{perturbed}$ for a particular perturbed equilibrium, using $\delta W_{perturbed}$ as the initial guess can improve convergence.

In contrast, when plasma equilibrium parameters, rather than wall parameters, were varied beyond a very narrow range of perturbations, the predicted stability $\delta W_{perturbed}$ consistently contained a large, rapidly growing error. We observed this error with perturbations to: the q profile for an experimental equilibrium, the aspect ratio for a simple equilibrium, and q profiles for a simple equilibrium. In all cases, the range of perturbations that gave acceptable results was very narrow.

Perturbing only the wall parameters is a useful application of the technique, but rather limited. The lure of drastically reduced computation time offered by the perturbative technique motivated us to understand and ameliorate the unexpected sensitivity

of toroidal stability to plasma equilibrium parameters. In Chapter 5 we explored several possible sources of the large error in $\delta W_{perturbed}$:

- Comparisons of various forms of $\omega^2 = \frac{\delta W}{K}$ verified that our mathematical expansion, matrix multiplication, and treatment of the vacuum energy are correct. These comparisons also indicated that ΔK slightly improves results, but does not appreciably reduce the rapid growth of the error in $\delta W_{perturbed}$.

- Inspection of the terms in the δW expansion indicated that second order terms are in fact quite large, and cannot be neglected.

- Comparison with NIMROD calculations and examination of equilibrium convergence, magnetic axis shifts, and mapping procedures gave us confidence that our equilibrium and coordinate system conversions do not contain inherent inconsistencies that might allow the second order terms to grow.

- Our assumption of small perturbations in the δW expansion is valid. Large variations that would have violated the premise of a perturbation expansion might have possibly accounted for the large second order terms.

- Investigation of the plasma energy components of δW associated the large second order terms with the fast compressional Alfvén energy. The terms of this component have relatively large coefficients that normally cancel when $\underline{\xi}$ is correct. Errors were not evident in the screw pinch analysis because the compressional Alfvén energy was analytically eliminated from δW.

- Attempts to estimate $\Delta\underline{\xi}$ with a simple minimization of the fast compressional Alfvén energy did not consistently reduce the error to an acceptable level. The error can occasionally be reduced when a reasonably insensitive parameter (such

as high aspect ratio) is perturbed. In general, however, correcting the fast compressional Alfvén energy transfers the error to other energy components.

- More rigorous minimizations of the fast compressional Alfvén energy might decrease the error, but would take more computation time than simply re-running the stability code and skipping the perturbation technique.

None of these efforts ultimately produced better estimates of δW. Changes in $\underline{\xi}$ must be considered as well, but are very difficult to estimate numerically. The stability eigenvalue problem $A\underline{x}\omega^2 = B\underline{x}$ is known to be sensitive to A and B [3], but we hoped that the sensitivity might be small enough to allow meaningful perturbations. Semi-analytic screw pinch equilibria and stability are rather robust, and do tolerate large perturbations, when the compressional Alfvén energy is eliminated from the analysis. Perturbing wall parameters with axisymmetric equilibria does not alter the plasma energy nor change the displacements in the bulk of the plasma, and therefore is also safe. But because of the precise cancellation required between large numbers, only infinitesimal perturbations to toroidal plasma equilibria are allowed.

Despite the extreme sensitivity of δW to changing plasma parameters, wall perturbations are still useful. Possible applications of the technique include optimizing wall distances to stabilize the resistive wall mode in tokamaks [42], developing novel wall cross-section shapes to stabilize the $n = 0$ vertical plasma displacement, quantifying the impact of wall parameters on edge-localized modes and investigating the effects of adding divertors, diagnostics, control systems, or other modifications to existing vessels.

Appendix A

Structure of Potential Energy Matrix A

The potential energy matrix A constructed by GATO and used in our perturbed calculations contains a $\psi \times \psi$ block diagonal of many $\theta \times \theta$ sparse sub-matrices, each with a central band. The central block diagonal band in each $\theta \times \theta$ sub-matrix contains further sub-matrices. These final 16×16 lower triangular sub-matrices contain the energy contributions. When only the fast compressional Alfvén energy (δW_{FCA}) contributes to the plasma energy in A, as described in Chapter 5, these lower triangular matrices resemble triangular checker boards.

If δW_{FCA} were the *only* contribution to A, the matrix structure would be vastly simplified. The $\theta \times \theta$ sub-matrices would be purely block diagonal, with some overlap to account for periodicity. However, the vacuum energy must also be retained for consistent boundary conditions. The vacuum energy is represented as a Green's function, with every point on the wall interacting with every point on the plasma surface. These important (θ_{wall}, $\theta_{surface}$) interactions account for the sparse off-diagonal elements.

Bibliography

[1] J.P.H.E. Ongena and G. Van Oost. *Transactions of Fusion Technology*, 33:9, March 1998.

[2] J.E. Menard, S.C. Jardin, S.M. Kaye, C.E. Kessel, and J. Manickam. *Nuclear Fusion*, 37(5):595, 1997.

[3] L.C. Bernard, F.J. Helton, and R.W. Moore. *Computational Physics Communications*, 24:377, 1981.

[4] A.D. Turnbull, M.S. Chu, T.S. Taylor, R.L. Miller, and Y.R. Lin-Liu. *Physics of Fluids B*, 4(10):3451, 1992.

[5] J. Candy, B.N. Breizman, J.W. Van Dam, and T. Ozeki. *Physics Letters A*, 215:299, 10 June 1996.

[6] H.A. Holties, J.P. Goedbloed, G.T.A. Huysmans, and W. Kerner. *Plasma Physics and Controlled Fusion*, 39:73, 1997.

[7] H.A. Holties, J.P. Goedbloed, G.T.A. Huysmans, W. Kerner, V.V. Parail, and F.X. Söldner. *Nuclear Fusion*, 36(8):973, 1996.

[8] G.T.A. Huysmans, J.P. Goedbloed, and W. Kerner. *Physics of Fluids B*, 5:1545, 1993.

[9] R.C. Grimm, J.M. Greene, and J.L. Johnson. In *Methods in Computational Physics*, volume 16, page 253, New York, 1976. Academic Press.

[10] J.A. Holmes, L.A. Charlton, J.T. Hogan, B.A. Carreras, and E.A. Lazarus. *Physics of Fluids B*, 1(2):358, 1989.

[11] A.D. Turnbull, M.S. Chu, T.S. Taylor, R.L. Miller, and Y.R. Lin-Lui. *Nuclear Fusion*, 38(10):1467, 1998.

[12] J.P. Freidberg. *Ideal Magnetohydrodynamics*. Plenum, New York, 1987.

[13] T.M. Antonsen and A. Bondeson. *Physics of Fluids B*, 5(11):4090, 1993.

[14] L.L. Lao, J.R. Ferron, R.J. Groebner, W. Howl, H. St.John, E.J. Strait, and T.S. Taylor. *Nuclear Fusion*, 30:1035, 1990.

[15] M. Mauel and L. Bai. In *Plasma Physics and Controlled Nuclear Fusion Research (Proc. 12th Int. Conf., Nice)*, volume 1, page 415, Vienna, August 1988. International Atomic Energy Agency.

[16] R.L. Miller and J.W. Van Dam. *Nuclear Fusion*, 27:2101, 1987.

[17] TOQ Grad-Shafranov equilibrium solver: `http://fusion.gat.com/toq`.

[18] H. Lütjens, A. Bondeson, and O. Sauter. *Computational Physics Communications*, 97:219, 1996.

[19] J. Delucia, S. Jardin, and A.J. Todd. *Journal of Computational Physics*, 37:183, 1980.

[20] H.P. Furth, J. Killeen, M.N. Rosenbluth, and B. Coppi. In *Plasma Physics and Controlled Nuclear Fusion Research*, volume 1, page 103, Vienna, 1965. International Atomic Energy Agency.

[21] J.M. Greene and J.L. Johnson. *Plasma Physics*, 10(8):729, 1968.

[22] G. Bateman. *MHD Instabilities*. MIT Press, Cambridge, Massacussetts, 1980.

[23] R. Gruber, F. Troyon, D. Berger, L.C. Bernard, S. Rousset, R. Schreiber, W. Kerner, W. Schneider, and K.V. Roberts. *Computational Physics Communications*, 21:323, 1981.

[24] R. Gruber and J. Rappaz. *Finite Element Methods in Linear Ideal Magnetohydrodynamics*. Springer-Verlag, Berlin, 1985.

[25] J.M. Greene and M.S. Chance. *Nuclear Fusion*, 21(4):453, 1981.

[26] C. Mercier and N. Luc. Technical Report EUR-5127e 140, Commission of the European Communities, Brussels, 1974.

[27] R.L. Miller, J.M. Greene, M.S. Chu, Y.R. Lin-Lui, and R.E. Waltz. *Physics of Plasmas*, 5(4):973, 1998.

[28] C.C. Hegna and N. Nakajima. *Physics of Plasmas*, 5(5):1336–1344, May 1998.

[29] S.R. Hudson, C.C. Hegna, R. Torasso, and A.S. Ware. *Plasma Physics of Controlled Fusion*, 46:869, April 2004.

[30] C.M. Bishop. *Nuclear Fusion*, 26:1063, 1986.

[31] C.M. Roach, J.W. Connor, and S. Janjua. *Plasma Physics and Controlled Fusion*, 37:679, 1995.

[32] L.E. Zakharov and B. Rogers. *Physics of Fluids B*, 4(10):3285, 1992.

[33] T.C. Hender et al. *Physics of Plasmas*, 6(5):1958, May 1999.

[34] J.A. Wesson. *Nuclear Fusion*, 18:87, 1978.

[35] T. Ozeki, M. Azumia, S. Tokuda, and S. Ishida. *Nuclear Fusion*, 33(7):1025, 1993.

[36] W. Kerner, P. Gautier, K. Lackner, W. Schneider, R. Gruber, and F. Troyon. *Nuclear Fusion*, 21:1383, 1981.

[37] B.A. Carreras et al. In *Proceedings of the 11th Conference on Plasma Physics and Controlled Fusion Research*, volume 2, page 53. Internation Atomic Energy Agency, 1987.

[38] W.A. Newcomb. *Annals of Physics*, 10:232, 1960.

[39] J.D. Callen, C.C. Hegna, B.W. Rice, E.J. Strait, and A.D. Turnbull. *Physics of Plasmas*, 6:2693, 1999.

[40] C.R. Sovinec, T.A. Gianakon, S.E. Kruger, D.D. Schnack, and E.D. Held. *Physics of Plasmas*, 10:1727, 2003.

[41] A.D. Turnbull, D.P. Brennan, M.S. Chu, L.L. Lao, J.R. Ferron, A.M. Garofalo, P.B. Snyder, J. Bialek, I.N. Bogatu, J.D. Callen, M.S. Chance, K. Comer, D.H. Edgell, S.A. Galkin, D.A. Humphreys, J.S. Kim, R.J. La Haye, T.C. Luce, G.A. Navratil, M. Okabayashi, T.H. Osborne, B.W. Rice, E.J. Strait, T.S. Taylor, and H.R. Wilson. *Nuclear Fusion*, 42:917–932, July 2002.

[42] A.M. Garofalo, A.D. Turnbull, M.E. Austin, J. Bialek, M.S. Chu, K.J. Comer, E.D. Fredrickson, R.J. Groebner, R.J. La Haye, L.L. Lao, E.A. Lazarus, G.A. Navratil, T.H. Osborne, B.W. Rice, S.A. Sabbagh, J.T. Scoville, E.J. Strait, and T.S. Taylor. *Physical Review Letters*, 82:3811, 1999.